

<sup>1</sup> **GLO-Roots: an imaging platform enabling multidimensional characterization of soil-grown ~~roots~~root systems**

<sup>3</sup> Rubén Rellán-Álvarez<sup>1, 9</sup>, Guillaume Lobet<sup>2</sup>, Heike Lindner<sup>1, 8</sup>, Pierre-Luc Pradier<sup>1, 8, 10</sup>,  
<sup>4</sup> Jose Sebastian<sup>1, 8</sup>, Muh-Ching Yee<sup>1</sup>, Yu Geng<sup>1, 7</sup>, Charlotte Trontin<sup>1</sup>, Therese LaRue<sup>3</sup>,  
<sup>5</sup> Amanda Schrager-Lavelle<sup>4</sup>, Cara H. Haney<sup>5</sup>, Rita Nieu<sup>6</sup>, Julin Maloof<sup>4</sup>, John P. Vogel<sup>7</sup>, José  
<sup>6</sup> R. Dinneny<sup>1, 12</sup>

<sup>7</sup> <sup>1</sup> Department of Plant Biology, Carnegie Institution for Science, Stanford, CA, USA.

<sup>8</sup> <sup>2</sup> PhytoSystems, University of Liège, Liège, Belgium.

<sup>9</sup> <sup>3</sup> Department of Biology, Stanford University, Stanford, CA, USA.

<sup>10</sup> <sup>4</sup> Department of Plant Biology, UC Davis, Davis, CA, USA.

<sup>11</sup> <sup>5</sup> Harvard Medical School, Massachusetts General Hospital, Department of Genetics, De-  
<sup>12</sup> partment of Molecular Biology Boston, MA, USA.~

<sup>13</sup> <sup>6</sup> USDA Western Regional Research Center, Albany, CA, USA.~

<sup>14</sup> <sup>7</sup> DOE Joint Genome Institute, Walnut Creek, CA, USA.~

<sup>15</sup> <sup>8</sup> These authors contributed equally

<sup>16</sup> <sup>9</sup> Present address: Laboratorio Nacional de Genómica para la Biodiversidad (Langebio),  
<sup>17</sup> Unidad de Genómica Avanzada, Centro de Investigación y de Estudios Avanzados del Instituto  
<sup>18</sup> Politécnico Nacional (CINVESTAV-IPN), Irapuato, Guanajuato, México

<sup>19</sup> <sup>10</sup> Present address: Boyce Thompson Institute for Plant Research/USDA, Ithaca, NY, USA.

<sup>20</sup> <sup>11</sup> Present address: Energy Biosciences Institute, UC, Berkeley, CA, USA

<sup>21</sup> <sup>12</sup> Corresponding author

<sup>22</sup> **Author contributions:**

<sup>23</sup> RR-A: Conception, design and development of the growth and imaging system and Arabidop-  
<sup>24</sup> sis transgenic lines; acquisition, analysis and interpretation of data; drafting and revising the

25 article.

26 GL: Development of the GLO-RIA image analysis plugin, analysis and interpretation of data,  
27 drafting and revising the article.

28 HL: Acquisition of data, development of the tomato growth and imaging setup.

29 P-LP: Acquisition of data, analysis and interpretation of data

30 JS: Development of Brachypodium transgenic lines, acquisition and analysis of Brachypodium,  
31 Arabidopsis and tomato data.

32 MCY: Development of Arabidopsis and Brachypodium transgenic lines.

33 YG: Development of Arabidopsis transgenic lines.

34 CT: Acquisition and analysis of the QPCR data

35 TL: Acquisition and analysis of the QPCR data

36 AS-L: Contributed the unpublished dual-color tomato line.

37 CH: Contributed the unpublished *Pseudomonas fluorescens* CH267-lux strain.

38 RN: Contribution to the development of the Brachypodium transgenic line.

39 JM: Contributed the unpublished dual-color tomato line.

40 JPV: Contribution to the development of the Brachypodium transgenic line.

41 JRD: Conception, design and development of the growth and imaging system and Arabidopsis  
42 transgenic lines; acquisition, analysis and interpretation of data; drafting and revising the  
43 article.

44 All authors read and approve the final version of the manuscript.

45 **Abstract**

46 Root systems develop different root types that individually sense cues from their local  
47 environment and integrate this information with systemic signals. This complex multi-  
48 dimensional amalgam of inputs enables continuous adjustment of root growth rates, direction

49 and metabolic activity that define a dynamic physical network. Current methods for  
50 analyzing root biology balance physiological relevance with imaging capability. To bridge  
51 this divide, we developed an integrated imaging system called Growth and Luminescence  
52 Observatory for Roots (GLO-Roots) that uses luminescence-based reporters to enable studies  
53 of root architecture and gene expression patterns in soil-grown, light-shielded roots. We  
54 have developed image analysis algorithms that allow the spatial integration of soil properties  
55 ~~such as soil moisture with root~~ and gene expression with root system architecture traits. We  
56 propose GLO-Roots as a system that has great utility in presenting environmental stimuli to  
57 roots in ways that evoke natural adaptive responses and in providing tools for studying the  
58 multi-dimensional nature of such processes.

## 59 Introduction

60 Plant roots are three-dimensional assemblies of cells that coordinately monitor and acclimate  
61 to soil environmental change by altering physiological and developmental processes through  
62 cell-type and organ-specific regulatory mechanisms<sup>1,2</sup>. Soil comprises a complex distribution  
63 of particles of different size, composition and physical properties, airspaces, variation in  
64 nutrient availability and microbial diversity<sup>3,4</sup>. These physical, chemical and biological  
65 properties of soil can vary on spatial scales of meters to microns, and on temporal scales  
66 ranging from seasonal change to seconds. Root tips monitor this environment through locally  
67 and systemically acting sensory mechanisms<sup>5,6</sup>.

68 The architecture of the root system determines the volume of soil where resources can be  
69 accessed by the plant (rhizosphere) and is under both environmental and genetic control.  
70 Plasticity in growth parameters allows the plant to adjust its form to suit a particular soil.  
71 Lateral roots, which usually make up the majority of the total root system, often grow at an  
72 angle divergent from the gravity vector. This gravity set-point angle (GSA) is controlled by  
73 auxin biosynthesis and signaling and can be regulated by developmental age and root type<sup>7</sup>.  
74 Recent cloning of the *DRO1* Quantitative Trait Locus (QTL) demonstrates that natural  
75 genetic variation is a powerful tool for uncovering such control mechanisms<sup>8</sup>.

76 Specific root ideotypes (idealized phenotypes) have been proposed to be optimal for acquisition  
77 of water and nitrogen, which are distinct from ideotypes for low phosphorus. Based on  
78 computational modeling and field studies, the “steep, deep and cheap” ideotype proposed by  
79 Lynch and colleagues may provide advantages to the plant for capturing water and elements  
80 like nitrogen that are water soluble and therefore tend to move in the soil column with water.  
81 This ideotype consists of highly gravitropic, vertically oriented roots that grow deep in the  
82 soil column and develop large amounts of aerenchyma, which reduces the overall metabolic  
83 cost of the root system<sup>3</sup>. Other nutrients, like phosphorus, which have limited water solubility  
84 and are tightly bound to organic matter, usually accumulate in the top layers of soil and favor  
85 roots systems that are more highly branched and shallow. The low-phosphorus ideotype  
86 effectively increases root exploration at the top layers of soil<sup>3</sup>. Modeling of root system  
87 variables shows that optimum architecture for nitrogen and phosphorus uptake are not  
88 the same<sup>9</sup> and suggests tradeoffs that may affect the evolution of root architecture as a  
89 population adapts to a particular environmental niche<sup>10</sup>.

90 Clearly, understanding the architecture of root systems and how environmental conditions  
91 alter root developmental programs is important for understanding adaptive mechanisms  
92 of plants and for identifying the molecular-genetic basis for different response programs.  
93 In addition, roots systems have complexity beyond their architecture that needs to be  
94 incorporated into our understanding of plant-environment interactions. Primary and lateral  
95 roots exhibit different stress response programs in *Arabidopsis*<sup>2,11</sup> and may play specialized  
96 roles in water and nutrient uptake. Thus, it is important to develop methods that allow for  
97 a multidimensional characterization of the root system that includes growth, signaling, and  
98 interactions with other organisms. Furthermore, physiological parameters that affect whole  
99 plant responses to the environment, such as transpiration, are likely integrated into such  
100 processes, thus requiring a more holistic approach to studies of root function.

101 Based on these considerations we have developed a new root imaging platform, Growth  
102 and Luminescence Observatory for Roots (GLO-Roots), which allows root architecture and  
103 gene expression to be studied in soil-grown plants. GLO-Roots is an integrated system

104 composed of custom growth vessels, luminescent reporters and imaging systems. We use  
105 rhizotrons that have soil volumes equivalent to small pots and support growth of Arabidopsis  
106 from germination to senescence. To visualize roots, we designed plant-codon optimized  
107 luciferase reporters that emit light of different wavelengths. To visualize reporter expression,  
108 plants are watered with a dilute luciferin solution and imaged afterwards. We have built a  
109 custom luminescence imaging system that automatically captures images of rhizotrons held  
110 vertically. The signal from each reporter is distinguished using band-pass filters held in a  
111 motorized filter wheel, which enables automated acquisition of images from plants expressing  
112 both structural and environmentally and developmentally responsive reporters. We have  
113 also developed GLO-RIA (GLO-Roots Image Analysis), an ImageJ<sup>1012</sup> plugin that allows  
114 for automated determination of (among other traits) root system area, convex hull, depth,  
115 width and directionality, which quantifies the angle of root segments with respect to gravity.  
116 GLO-RIA is also able to relate root system parameters to local root-associated variables  
117 such as reporter expression intensity and soil-moisture content.

118 Overall GLO-Roots has great utility in presenting environmental stimuli to roots in physio-  
119 logically relevant ways and provides tools for characterizing responses to such stimuli at the  
120 molecular level in whole adult root systems over broad time scales.

## 121 **Box 1.**

122 All resources for GLO-Roots, including the original raw data used in the manuscript, sample  
123 images, GLO-RIA user manual, the latest software updates and the source code, can be  
124 found at: <https://dinnenylab.wordpress.com/glo-roots/>

## 125 **Results.**

126 We have developed an integrated platform for growing, imaging and analyzing root growth  
127 that provides advances in physiological relevance and retains the ability to visualize aspects  
128 of root biology beyond structure.

<sup>129</sup> **The GLO-Roots ~~plattform~~platform.**

<sup>130</sup> GLO-Roots is comprised of four parts: i) growth vessels called rhizotrons that allow plant  
<sup>131</sup> growth in soil and root imaging; ii) luminescent reporters that allow various aspects of root  
<sup>132</sup> biology to be tracked in living plants; iii) GLO1 luminescence-imaging system designed to  
<sup>133</sup> automatically image rhizotrons; iv) GLO-RIA, an image analysis suite designed to quantify  
<sup>134</sup> root systems imaged using GLO-Roots.

<sup>135</sup> **Plant growth system.** GLO-Roots utilizes custom designed growth vessels classically  
<sup>136</sup> known as rhizotrons, which hold a thin volume of soil between two sheets of polycarbonate  
<sup>137</sup> plastic. Acrylic spacers provide a 2-mm space in which standard peat-based potting mix is  
<sup>138</sup> added. Black vinyl sheets protect roots from light and rubber U-channels clamp the rhizotron  
<sup>139</sup> materials together. Plastic racks hold the rhizotrons vertically and further protect the roots  
<sup>140</sup> from light. Rhizotrons and rack are placed in a black tub and water ~~are~~is added, to a depth  
<sup>141</sup> of about 2 cm, at the bottom to maintain moisture in the rhizotrons during plant growth.  
<sup>142</sup> The volume of soil in the rhizotrons ( $100 \text{ cm}^3$ ) is similar to small pots commonly used for  
<sup>143</sup> Arabidopsis and supports growth throughout the entire life cycle (Fig 1A-C and Supplement  
<sup>144</sup> 1).

<sup>145</sup> To determine how the biology of plants grown in rhizotrons compares to other standard  
<sup>146</sup> growth systems, we utilized high-throughput qRT-PCR to study how these conditions affect  
<sup>147</sup> expression of 77 marker genes in root and shoot samples. These genes were curated from the  
<sup>148</sup> literature and belong to a wide array of biological pathways including nutrient acquisition,  
<sup>149</sup> hormone and light response and abiotic stress. Whole roots and shoot samples were collected  
<sup>150</sup> at the end of the light and dark periods (Long-day conditions: 16 hour light, 8 hours dark)  
<sup>151</sup> from plants grown in rhizotrons, pots, and petri dishes with two different media compositions~~(~~1  
<sup>152</sup> 1X Murashige and Skoog basal salts (~~MS~~1~~ms~~) 1% sucrose or 0.25X ~~MS~~1~~ms~~, no sucrose  
<sup>153</sup> (ms25). Principal component analysis of the gene expression values showed a separation of soil  
<sup>154</sup> and gel-grown root systems in the the first principal components (Figure 1-figure supplement  
<sup>155</sup> 1A). In roots grown on gel-based media, we observed enhanced expression of genes associated

156 with light-regulated pathways (flavonoid biosynthesis: *FLAVINOL SYNTHASE1*, *FLS1*,  
157 *CHALCONE SYNTHASE*, *CHS* and photosynthesis: *RUBSICO SUBUNITS1A*~~RUBISCO~~  
158 *SUBUNIT 1A*, *RBCS1A*, *CYCLOPHILIN 38*, *CYP38*), which is expected due to the  
159 exposure of gel-grown roots to light. In addition, genes associated with phosphorus nutrition  
160 (*LOW PHOSPHATE RESPONSE1*, *LPR1*, *PHOSPHATE STARVATION RESPONSE1*,  
161 *PHR1*) were (Figure 1-figure table supplement 1) less expressed in soil-grown roots, suggesting  
162 differences in nutrient availability between the different growth systems. Interestingly, shoot  
163 samples where not ~~clearly distinguished~~as clearly separated by growth media and, instead,  
164 time of day had a greater effect (Figure 1-Supplement 2). These data suggest root systems  
165 may be particularly sensitive to media conditions and indicate that rhizotron-grown root  
166 systems more closely approximate the biology of pot-grown plants than standard gel-based  
167 media. Shoot weight and primary root length were significantly reduced for gel-grown plants  
168 compared to rhizotron- or pot-grown plants suggesting significant differences in the biology  
169 of plants grown under these conditions (Figure 1-figure supplement 1B-C).

170 While the 2 mm depth of the soil sheet is 10 to 20 times the average diameter of an Arabidopsis  
171 root (between 100-200 microns<sup>4413</sup>), we evaluated whether rhizotron-grown plants exhibited  
172 any obvious stress as a consequence of physical constriction. We compared traits of plants  
173 growing in vessels that hold similar volumes of soil but in different volumetric shapes. The  
174 number of lateral roots was significantly lower in pot and cylinder-grown plants compared  
175 to rhizotron-grown plants (Figure 1-figure supplement 1D) whereas primary root length of  
176 rhizotron and cylinder-grown plants was significantly greater than pot-grown plants (Figure  
177 1-figure supplement 1E). No significant differences in shoot area were observed between the  
178 three systems (Figure 1-figure supplement 1-data). Thus, these data do not support the  
179 hypothesis that rhizotron-grown plants experience physical constriction greater than other  
180 vessels holding the same volume of soil.

181 **Generation of transgenic plants expressing different luciferases.** Arabidopsis roots  
182 cannot easily be distinguished from soil using brightfield imaging due to their thinness and  
183 translucency (Figure 1-figure supplement 3); thus, reporter genes are needed to enhance the

184 contrast between the root and their environment. Luciferase is an ideal reporter to visualize  
185 roots: 1) unlike fluorescent reporters, luciferase does not require high-intensity excitation  
186 light, which could influence root growth, 2) peat-based soil (a type of histosol) exhibits no  
187 autoluminescence but does autofluoresce at certain excitation wavelengths similar to GFP  
188 (Figure 1-figure supplement 3), 3) while GFP is very stable, and thus not as suitable for  
189 imaging dynamic transcriptional events, the luciferase enzyme is inactivated after catabolism  
190 of luciferin, making it ideal for studying processes such as environmental responses. A  
191 considerable number of luciferases have been developed that emit light spanning different  
192 regions of the visible spectrum, but their utilization has been limited to studies in animals  
193 (Table 1).

194 To determine the efficacy of using luciferase to visualize roots in soil, we codon optimized  
195 sequences of *PpyRE8*, *CBGRed*, *LUC2*, and *CBG99* for Arabidopsis expression. In addition,  
196 nanoLUC<sup>14</sup> and venus-LUC2<sup>4215</sup> were utilized. Constitutive luciferase expression was driven  
197 in plants using the *UBIQUITIN 10* (*UBQ10*) or *ACTIN2* (*ACT2*) promoters using vectors  
198 assembled through a Golden-Gate cloning system<sup>4216</sup>. Plants homozygous for a single locus T-  
199 DNA insertion were evaluated for in vivo emission spectra and luminescence intensity (Fig 1D).  
200 All the evaluated luciferases use D-luciferin as a substrate facilitating the simultaneous imaging  
201 of different luciferases except nanoLUC, which uses a proprietary substrate furimazine<sup>14</sup>. **In**  
202 **general, luciferases Luciferases** with red-shifted emission spectra were less intense than the  
203 green-shifted luciferases (Fig 1D). LUC2o showed an emission maximum at 580 nm and a  
204 minor peak at 620 nm while CBG99o lacks the minor peak.

205 Continuous addition of luciferin did not have any significant effect on shoot weight or primary  
206 root length (Figure 1-figure supplement 4). After luciferin addition, luminescence signal  
207 could be reliably detected in root systems for up to 10 days, depending on the developmental  
208 state of the plant.

209 **GLO1: a semi-automated luminescence imaging system for rhizotrons.** Lumines-  
210 cence imaging systems commercially available for biomedical research are usually optimized

for imaging horizontally held specimens or samples in microtiter plates. Placing rhizotrons in this position would induce a gravitropic response in plants. Working with Bioimaging Solutions (San Diego, CA) we designed and built a luminescence imaging system optimized for rhizotron-grown plants. GLO1 (Growth and Luminescence Observatory 1) uses two PIXIS-XB back-thinned CCD cameras (Princeton Instruments, Trenton, NJ, USA) to capture partially-overlapping images of rhizotrons while a motorized stage automatically rotates the rhizotron to capture images of both sides (Fig 1E). A composite image is generated from the images captured of each side; Fig 1F shows that approximately half of the root system is revealed on each side with few roots being visible on both sides. Apparently, the soil sheet is thick enough to block portions of the root system but thin enough to ensure its continuous structure can be compiled from opposite face views. We tested the ability of GLO1-generated images to reveal complete root systems by manually quantifying the number of lateral roots in excavated root systems of 8 different plants and testing these results against estimates of lateral root number from images of the same plants visually inspected by 4 different persons. These comparisons revealed good correlation ( $(R^2 = 0.974)$ ) between actual lateral root counts and image-based estimation, indicating GLO1-generated root images provide an accurate representation of the in soil root system.

**GLO-RIA: GLO-Roots Image Analysis.** We developed a set of image analysis algorithms that were well suited for the complex root systems that GLO-Roots is able to capture. GLO-RIA (Growth and Luminescence Observatory Root Image Analysis) is an ImageJ plugin divided in two modules. The first module (RootSystem) performs four different types of analysis: i) a local analysis that detects all root particles in the image and computes their position, length and direction; ii) the global analysis performs a root system level analysis and computes the total visible surface, convex hull, width and depth; iii) the shape analysis uses Elliptic Fourier Descriptors or pseudo-landmarks similarly to RootScape<sup>45,17</sup> to perform a shape analysis on the root system iv) the directionality analysis computes the mean direction of root particles in a root system (either on the full image or by a user-defined region of interest in the image).

239 These four analysis methods are fully automated by default, but can be manually adjusted if  
240 needed.

241 The second module of GLO-RIA (RootReporter) was specifically designed for the analysis of  
242 multi-layered images such as combinations of gene reporter, root structure and soil moisture.  
243 Shortly, the plugin works as follows: i) detection of the gene reporters and the structure  
244 reporters in their respective images; ii) if needed, a manual correction can be performed to  
245 correct the automated detection; iii) gene reporters are linked with the soil water content  
246 and the structure reporters, based on their proximity; iv) gene reporter intensity (either  
247 absolute or normalized using the structural reporter) is computed; v) all data are exported  
248 and saved to a [RSML datafile](#)[Root System Markup Language \(RSML\) datafile<sup>1618</sup>](#). Gene  
249 and structure reporters can be followed across different time and space points. Using  
250 an object oriented approach, great care has been taken to facilitate the user interactions  
251 on the different images to streamline the analysis process. Table 2 shows a list of root  
252 system features extracted using GLO-RIA. GLO-RIA does not currently have the ability  
253 to reconstruct the root architecture in itself (topological links between roots). This is a  
254 challenge for analyzing images captured by GLO-Roots since soil particles cause disruption  
255 of root segments.

256 [We tested the accuracy of the measurements obtained from GLO-RIA using two different](#)  
257 [ground-truthed data sets. Manual measurement of root system width, depth and average](#)  
258 [lateral root angle was determined by hand using imageJ from an independent set of images](#)  
259 [corresponding to roots of several Arabidopsis accessions growing in control conditions. We](#)  
260 [also used ArchiSimple<sup>19</sup> to generate 1240 images of root system models with contrasting](#)  
261 [sizes and lateral root angles. Since these images are computationally generated, exact](#)  
262 [determination of root system parameters was possible. For both ground truth data](#)  
263 [sets, GLO-RIA quantification provided measurements that were well correlated for all](#)  
264 [all three measured parameters \(Figure 1-figure supplement 5D-F\). Sample images of](#)  
265 [real and ArchiSimple generated root images shown with GLO-RIA-defined directionality](#)  
266 [color-coding \(Figure 1-figure supplement 5G-I\).](#)

**267    Continuous imaging of root growth.**

**268** The size of our rhizotrons enables undisturbed root system development (before roots reach  
**269** the sides or the bottom of the rhizotron) for about 21-23 days for the Col-0 accession  
**270** growing under long day conditions (Figure 2); however root traits such as directionality  
**271** can be observed through later stages of plant development. See 35 DAS root system and  
**272** directionality in Figure 2A-B. An example of a time series spanning 11 to 21 days after  
**273** sowing (DAS) of Col-0 roots expressing *ProUBQ10:LUC2o* is shown in Fig 2A and [Video 1](#)  
**274** with a color-coded time projection shown in Fig 2C. Directionality analysis (Fig 2B) shows a  
**275** progressive change in root system angles from  $0^{\circ}$ - $0^{\circ}$  (vertical) to  $45^{\circ}$ - $45^{\circ}$  as lateral roots  
**276** take over as the predominant root type. Figure 2D shows the evolution over time of several  
**277** root traits that can be automatically captured by GLO-RIA (depth, width, area) and others  
**278** that were manually quantified (primary root growth rate or number of lateral roots per  
**279** primary root).

**280    Root system architecture of different *Arabidopsis* accessions.**

**281** As a proof of concept to estimate the utility of our root imaging system to phenotype  
**282** adult root system traits, we transformed a small set of accessions (Bay-0, Col-0 and Sha)  
**283** with the *ProUBQ10:LUC2o* reporter and quantified RSA at 22 DAS (Fig 3A-C). GLO-RIA  
**284** analysis of these root systems identified several root traits that distinguish Col-0, Bay-0  
**285** and Sha. Directionality analysis revealed an abundance of steep-angle regions in the root  
**286** system of Bay while Sha showed an abundance of shallow-angled regions and Col-0 was  
**287** intermediate (Fig 3D). Bay-0 shows the deepest and narrowest root system leading to the  
**288** highest depth/width ratio while Sha has the widest root system (Fig 3E). Other root traits  
**289** such as root system area and the vertical center of mass also showed significant differences  
**290** (Figure 3-figure supplement 1B). Broad sense heritability values for depth (96.3), area (92.0),  
**291** depth/width (97.8), width (95.7) and vertical center of mass (95.0) were all higher than 90%.  
**292** To capture the richness of root architecture shape, we used GLO-RIA to extract pseudo-  
**293** landmarks describing the shape of the root system (see Materials and Methods for more

294 details) and performed PCA analysis. The first principal component captures differences in  
295 the distribution of widths along the vertical axis and separates Col-0 and Sha from Bay-0  
296 root systems. (Fig 3F). Bay-0 shows an homogenous distribution of widths along the vertical  
297 axis while Sha and Col-0 are much wider at the top than bottom. PC2 seems to be capturing  
298 a relationship between width at the top and total depth and separates Sha root systems  
299 which are wide at the top and deep from Col-0 root systems which are wide but not as  
300 deep as Sha. Shape information extracted from pseudo-landmarks can distinguish the three  
301 different accession using PCA analysis (Fig 3G).[~](#)

302 **Spectrally distinct luciferases enable gene expression patterns, characterization**  
303 **of root system interactions and microbial colonization.**

304 We tested whether spectrally distinct luciferase reporters would enable additional information  
305 besides root architecture to be captured from root systems. Luciferase reporters have been  
306 commonly used to study gene expression and these resources can potentially be utilized to  
307 study such regulatory events in soil-grown roots. We transformed *ProACT2:PpyRE8o* into  
308 two well studied LUC reporter lines: the auxin response reporter line *ProDR5:LUC*<sup>+1720</sup>  
309 (Figure A-B) and the Reactive Oxygen Species (ROS) response reporter *ProZAT12:LUC*<sup>+1821</sup>  
310 (Figure 4C-D). We implemented in GLO-RIA an algorithm that semi-automatically identifies  
311 gene reporter signal and associates this object to the corresponding root structure segment.  
312 A graphical representation of the results obtained with Root Reporter can be observed in  
313 Figure 4-figure supplement 1. Reporter intensity values along the first 5 mm of root tips can  
314 also be observed in Figure 4-figure supplement 2.  
315 We then took advantage of our ability to constitutively express two spectrally different  
316 luciferases and imaged the overlapping root systems (one expressing *ProUBQ10:LUC2o* and  
317 the other *ProACT2:PPy RE8o*). While two root systems were distinguishable using this  
318 system (Figure 4-figure supplement 3); measurements of root system area did not reveal a  
319 significant effect on root growth when two plants were grown in the same rhizotron, compared  
320 to one; however, further studies are warranted (Figure 4-figure supplement 3).

321 The GLO-Roots system uses non-sterile growth conditions, which allows complex biotic  
322 interactions that may affect responses to the environment. Bacteria themselves can be  
323 engineered to express luminescent reporters through integration of the LUX operon, which  
324 results in luminescence in the blue region of the spectrum and is thus compatible with the  
325 plant-expressed luciferase isoforms we have tested. *Pseudomonas fluorescens* CH267<sup>1922</sup>,  
326 a natural *Arabidopsis* root commensal, was transformed with the bacterial LUX operon  
327 and used to inoculate plants. Thirteen days after inoculation, we were able to observe  
328 bacterial luminescence colocalizing with plant roots. *P. fluorescens* did not show an obvious  
329 pattern of colonization at the root system scale level. As a proof-of-principle test of the  
330 multi-dimensional capabilities of the GLO-Roots system we visualized both *LUC2o* and  
331 *PPyRE8o* reporters in plants and the LUX reporter in bacteria in the same rhizotron (Figure  
332 4-figure supplement 4).

333 **Adaptive changes in root system architecture under water deprivation, phos-**  
334 **phorus deficiency and light.** To test the utility of the GLO-Roots system to understand  
335 response of root systems to environmental stimuli we tested the effects of light and conditions  
336 that mimic drought and nutritional deficiency. To examine the effects of light exposure on  
337 the root architecture, the black shields, which normally protect the soil and roots from light,  
338 were removed from the top half of the rhizotrons 10 DAS. Using directionality analysis we  
339 detected a significant increase in the steepness of roots only in the light exposed region of  
340 the rhizotron, while the lower shielded region showed no difference. (Fig 6-figure supplement  
341 3A-B and Fig 6-figure supplement 4). Light can penetrate the top layers of soil<sup>2023</sup> and it  
342 has been proposed to have a role in directing root growth specially in dry soils<sup>2124</sup> through  
343 the blue light receptor *phot1*. Root directionality was not significantly different between light  
344 and dark-treated roots of the *phot1/2* double mutant suggesting that blue light perception  
345 is necessary for this response<sup>2124,2225</sup> (Fig 6-figure supplement 3B-lower panel). These  
346 data highlight the strong effects of light on root system architecture<sup>2326</sup>, which GLO-Roots  
347 rhizotrons are able to mitigate.

348 Plants grown in low-P soil showed a significant increase in the width-depth ratio of the root

349 system compared to plants grown in P-replete soil, as determined using the automated root  
350 system area finder in GLO-RIA (Fig 6-figure supplement 2A-B). Plants under P deficiency  
351 showed an increase in the ratio between root-shoot area (Fig 6-figure supplement 2C) and  
352 higher investment of resources in the development of the root system at the expense of  
353 shoot growth (Fig 6-figure supplement 2D). Root systems of control and P-deficient plants  
354 showed no significant differences in directionality at 22 DAS but at 27 DAS, roots were more  
355 horizontally oriented in P-deficient plants (Fig 6-figure supplement 2E). The observed changes  
356 in root architecture are consistent with root system ideotypes that improve phosphorus  
357 uptake efficiency.

358 GLO-Roots is especially well suited for studying water-deficit (WD) responses. First, shoots  
359 are exposed to the atmosphere and vapor pressure deficit (**VPD**) is maintained at levels that  
360 allow for transpiration of water from the shoot. Second, soil in rhizotrons is exposed to  
361 air at the top and dries **basipetally** (from the top-down); drying soil increases the volume  
362 occupied by air and reduces contact of root with liquid water, all of which are similar to  
363 changes in soil expected in the field during WD. Finally, as peat-based soil dries, its optical  
364 properties change, allowing moisture content to be approximated from bright-field images.  
365 We took advantage of the change in gray-scale pixel intensity to construct a calibration  
366 curve (Figure 5-figure supplement 1) that quantitatively relates gray-scale pixel intensity to  
367 moisture content (Fig 5A); water content can be color coded in images with appropriate look  
368 up tables (Fig 5B). Soil color was not affected by the presence or absence of roots (Figure  
369 5-figure supplement 2). Using this approach, water content in a rhizotron can be mapped  
370 and visualized in 2D (Fig 5C-D). In the example shown, we can observe that a 22 DAS Bay-0  
371 plant depleted soil-moisture content locally around the **the** root system (Figure 5E).

372 We performed several trials to simulate WD in our growth system. Plants were germinated,  
373 grown under control conditions then transferred to 29°C and standing water removed from  
374 the container holding the rhizotrons starting at 9 DAS or 13 DAS. Elevated temperature  
375 combined with water deficit is a common stress that modern crops varieties are poorly  
376 adapted to, thus highlighting the importance of examining this combined treatment<sup>24,27,25,28</sup>.

377 Plants were maintained in this WD regime until 22 DAS when luciferin solution was added  
378 and the plants imaged. At 13 DAS, lateral roots near the soil surface are already emerged  
379 ([Video 1](#), Figure 2A) and 9 days of subsequent WD treatment caused lateral roots to show an  
380 increase in gravitropism leading to the development of a root system that were deeper and  
381 more vertically oriented (Fig 6A). Roots of Bay-0 plants showed similar responses, though  
382 the extent of change was less pronounced since Bay-0 roots are normally more vertically  
383 oriented (Fig 6B). Plants transferred at 9 DAS and grown for 13 days under WD showed less  
384 lateral root development in the top layer of soil (Fig 6E). At this time point, lateral roots  
385 start to emerge ([Video 1](#)) and early drought may lead to growth quiescence or senescence.  
386 Careful examination of roots in these regions showed evidence of small lateral root primordia  
387 populating the primary root (Figure 6F). After 24 h of re-watering (Figure 6G) these lateral  
388 root primordia reinitiated growth (Figure 6H).

389 Time-lapse imaging of the water deficit response showed that changes in root growth direction  
390 occurred ahead of the dry soil front [Video 2](#). Using GLO-RIA we were able correlate local  
391 water moisture contents with the orientation of root segments. With this approach we  
392 observed that root segments in dryer areas of rhizotron grew at steeper root angles (Figure  
393 7) than roots in WW regions, though lateral root angle in wetter regions was also affected.  
394 These data suggest that both local and systemic signaling is likely involved in redirecting  
395 lateral roots deeper during the simulated drought treatments tested here.

396 We also grew plants under WD at control temperatures or under WW conditions at elevated  
397 temperature to test the effects of these individual stresses on root architecture. We observed  
398 that both conditions were sufficient to induce a change in root directionality indicating that  
399 the plant uses similar mechanisms to avoid heat and water-deficit associated stresses (Figure  
400 6-figure supplement 1). We next asked which regulatory pathways controlled the observed  
401 changes in lateral root directionality during simulated drought. Hydrotropism is a known  
402 environmental response that directs root growth towards wet regions of soil. MIZ1 is an  
403 essential regulator of hydrotropism; however *miz1* mutants had no significant effect on water  
404 deficit-induced changes in root directionality, compared to wild type (Fig 6C), indicating

405 that this response was distinct from hydrotropism. Auxin is an important mediator of  
406 gravitropism and auxin treatment causes lateral roots to grow more vertically<sup>7</sup>. Consistent  
407 with this role for auxin, mutant plants with loss of function in the auxin receptor TIR1, did  
408 not show changes in the root system directionality between WW and WD conditions (Fig  
409 6D).

410 **GLO-Roots for Brachypodium and Tomato.**

411 To examine the general applicability of the GLO-Roots system for other species, we introduced  
412 LUC2o-expressing reporters into the model grass *Brachypodium distachyon* and the crop  
413 plant *Lycopersicon esculentum* (tomato). Brachypodium is well suited to the GLO-Root  
414 system because, like Arabidopsis, its small size allows mature root systems to be studied in  
415 relatively small soil volumes<sup>2629,2730</sup>. *LUC2o* driven by the *ZmUb1* promoter was introduced  
416 into Brachypodium using the pANIC vector<sup>2831</sup>. Brachypodium roots showed a distinct  
417 architecture from Arabidopsis marked by prolific development of secondary and tertiary  
418 lateral roots (Fig 8A). This is consistent with other studies that show that Brachypodium  
419 has a typical grass root system<sup>2730</sup>. Comparison of root system development in rhizotrons  
420 with gel-based media showed that root growth is higher in soil than in plates (Figure 8-figure  
421 supplement 1). Previous work has suggested that auxin levels in Brachypodium roots is sub-  
422 optimal for growth<sup>2932</sup>. Pacheco-Villalobos and colleagues suggest that, in Brachypodium,  
423 and contrary to what happens in Arabidopsis, ethylene represses *YUCCA* reducing the  
424 synthesis of auxin. The reduced growth that we observe in plates and the high levels of  
425 ethylene that build up in sealed plates<sup>3033</sup> would support this mechanism.

426 Tomato plants were transformed with *Pro35S:PPyRE8o* and *ProeDR5rev:LUC2* reporters.  
427 The plants showed more rapid growth than Arabidopsis or Brachypodium and required  
428 fertilizer to prevent obvious signs of stress (reduced growth, anthocyanin accumulation).  
429 Root systems were imaged from 17 DAS plants. Roots showed presumptive lateral root  
430 primordia marked by DR5-expression (Fig 8C-D). These results show that the GLO-Roots  
431 method can be applied to study root systems of plants and will likely be useful for studying

432 root systems of other small to medium sized model plants and for early stages of larger crop  
433 plants.

434 **Discussion.**

435 **GLO-Roots enables a multi-dimensional understanding of root biology.**

436 Recent studies of root systems has emphasized structural attributes as important contributors  
437 of root system function. Indeed, studies examining the role of genetic variants in tolerating  
438 abiotic stress have demonstrated the importance of such characteristics<sup>8</sup>. Roots, however,  
439 are highly diverse in the biology they perform and a multi-dimensional understanding of root  
440 systems, which incorporates differences in signaling, metabolism and microbial association  
441 as well as structure, may provide a clearer understanding of the degree to which sub-  
442 functionalization of the root system plays a role in important processes such as acclimation  
443 and efficient resource acquisition.

444 We have developed tools in GLO-Roots that allow for tracking multiple aspects of soil  
445 physicochemical properties and root biology simultaneously. Using GLO-Roots, we are able  
446 to map in 2D coordinates soil physical properties such soil moisture together with root  
447 architecture traits such as directionality, growth rates and gene expression levels. All this  
448 information is aggregated in layers for each x, y coordinate. Using GLO-RIA we integrate this  
449 multilayer information, leveraging our ability to simultaneously and seamlessly investigate  
450 root responses to environmental stimuli such as soil moisture content. **Luciferase isoforms**  
451 **Luciferases** that emit light at different wavelengths allow for constitutive and regulated  
452 promoters to be studied together. Introduction of luciferase reporters into microbes provides  
453 an additional layer of information that provides a readout on the association between  
454 organisms and how this might be affected by environmental conditions. The flexibility  
455 of the GLO-Roots system may enable additional dimensionality to our understanding of  
456 root biology. Other physical properties such as CO<sub>2</sub> or pH mapping in rhizotrons have  
457 already been enabled by using planar optodes<sup>34,35</sup>. It may be possible to engineer LUX-based

458 reporters in microbes that are responsive to extracellular metabolites, creating microbial  
459 biosensors, and integration of such tools may enable root-exudation and nutrition to be  
460 analyzed in soil. Split-Luciferase reporters have been engineered that allow bi-molecular  
461 interactions to be studied. Finally, molecular sensors analogous to FRET sensors, termed  
462 BRET-sensors<sup>3235</sup>, may allow metabolite tracking dynamically through the root system.  
463 With additional innovation in the development of luciferase reporters, the GLO-Roots systems  
464 will likely expand the repertoire of biological processes that can be studied over an expanded  
465 range of developmental time points and environmental conditions.

466 **Enhanced root growth and gravitropism may constitute an avoidance mechanism  
467 used during water deficit stress.**

468 It has been proposed that plants with steep root systems will be better able to tap into deep  
469 water resources and thus perform better under water deprivation. For example in rice, the  
470 IR64 paddy cultivar shows shallow root systems in upland fields whereas Kinandang Patong,  
471 an upland cultivar, is deeper rooting<sup>8</sup>. Plants maintain a number of regulatory pathways  
472 that mediate changes in physiology during WD. Enhanced growth of root systems has been  
473 well characterized in field-grown plants; however this has not been recapitulated in studies of  
474 gel-grown Arabidopsis plants. Thus, it has been unclear whether Arabidopsis simply responds  
475 to WD differently. Our results here show that Arabidopsis does indeed maintain a classical  
476 WD response that expands the root system and directs growth downward. Interestingly,  
477 under our stress regime, we did not observe a significant decrease in the relative water  
478 content of shoot tissues (Figure 6-figure supplement 5), suggesting that the changes in root  
479 architecture were sufficient to provide access to deep water and prevent dehydration. Such  
480 changes in root growth are likely regulated through systemic and local signaling that involve  
481 auxin signaling but acts independently of known pathways that control moisture-directed  
482 root growth.

**483 Perspectives and Conclusions.**

484 Understanding plant biology requires a sophisticated understanding of how environmental  
485 stimuli affect the form and function of plants as well as an understanding of how physiological  
486 context informs such responses. Environmental conditions are at least as complex as the  
487 plants they affect. Plant roots are exposed to a variety of environmental signals that change  
488 in time and space at very different scales that are integrated at the whole plant system. It is  
489 an important challenge in biology to develop methods of growing and studying plants that  
490 present such stimuli in a manner that the plant is likely to encounter in nature. After all, the  
491 plants we study have evolved to survive through mechanisms that have been selected, over  
492 evolutionary time, in nature. It will be interesting for future studies to determine how other  
493 environmental stimuli affect root growth using GLO-Roots and whether these responses  
494 differ between accessions of Arabidopsis. Identification of the genetic loci responsible for  
495 phenotypic variation in adult root phenotypes may identify the molecular basis for adaptive  
496 variation that exists in this species and potentially identify loci that are useful for breeding  
497 efforts needed for the next green revolution.

**498 Materials and methods.**

**499 Growth system.**

500 **Rhizotrons and growth system fabrication.** Rhizotrons are composed of two sheets of  
501 1/8" abrasion resistant polycarbonate plastic (Makrolon AR (R)) cut to size using a water  
502 jet (AquaJet LLC, Salem, OR), two acrylic spacers cut using a laser (Stanford Product  
503 Realization Lab), two rubber U-channels cut to strips 30 cm long ([McMaster Carr part #](#)  
504 [8507K33](#)) and two sheets of black 0.030" thick polypropylene sheets ([McMaster Carr part #](#)  
505 [1451T21](#)) cut with a straight-edge razor blade. Rhizotron designs were drafted in Adobe  
506 Illustrator (Adobe, San José, CA). The blueprints of all the parts are provided in Supplement  
507 1. The top edge of each polycarbonate sheet was painted with black 270 Stiletto nail polish  
508 (Revlon, New York, NY).

509 **Boxes and holders.** Rhizotrons are held vertical during plant growth in a custom rack  
510 system composed of two sheets of 1/4" black acrylic plastic cut with slots for eleven rhizotrons  
511 using a laser, four 3/8" PVC rods ([McMaster Carr part # 98871a041](#)) secured with PVC  
512 nuts ([McMaster Carr part # 94806a031](#)) to hold the acrylic sheets horizontal. The rack is  
513 placed inside a 12" x 12" x 12" black polyethylene tank ([Plastic Mart part # R121212A](#)).

514 **Rhizotron preparation** The procedure to construct a rhizotron with soil is as follows:  
515 Two pieces of polycarbonate plastic are laid flat on a table with the spacers inserted. Using  
516 an electric paint gun, a fine mist of water is applied to the bare polycarbonate sheets. Then,  
517 using a 2 mm sieve (US Standard Sieve Series N° 10) a fine layer of PRO-MIX(r) PGX soil  
518 (Premier Tech, Canada) is applied. Excess soil is discarded by gently tapping the plastic  
519 against the table in a vertical position. Water is sprayed again onto the soil, then a second  
520 layer of Pro-MIX is applied as before. For P deficiency experiments soil supplemented with 1  
521 ml of 100 µM P-Alumina (control) and 0-P-Alumina (P deficient ) was used. To prevent the  
522 soil from falling out of the bottom opening, a 3 x 6 cm piece of nylon mesh is rolled into a 1  
523 cm wide tube and placed at the bottom side of the rhizotron. The spacers are removed and  
524 replaced by clean spacers. The two faces of the rhizotron are carefully joined together and  
525 two rubber U-channels slipped on to clamp all pieces together. Assembled rhizotrons are  
526 placed into the rack inside the boxes and 500 mL of water is added to the box.

527 **Plant growth** *Arabidopsis thaliana* seeds were stratified for 2 d at 4 °C in Eppendorf tubes  
528 with distilled water. Seeds were suspended in 0.1 % agar and 5 to 10 were sown using a  
529 transfer pipette in the rhizotron. A transparent acrylic sheet was mounted on top of the box  
530 and sealed with tape to ensure high humidity conditions that enable *Arabidopsis* germination.  
531 Three days after sowing, the cover was unsealed to decrease humidity and allow the seedlings  
532 to acclimate to a dryer environment. From 3 days after sowing (DAS) to the time the first  
533 true leaves emerged, it was critical to ensure that the top part of the rhizotron remained  
534 humid for proper germination of the plants. Between three and five DAS the rhizotrons  
535 were thinned leaving only the number plants required for that experiment, typically one,  
536 except for experiments examining root-root interactions. Unless otherwise stated, all the

537 experiments presented here, treatments were started 10 DAS. Plants were grown under long  
538 day conditions (16 h light / 8 h dark) using 20–22 °C (day/night) and 150 µE m<sup>-1</sup> s<sup>-1</sup>. Two  
539 types of growth environments were used for experiments. A walk-in growth chamber with  
540 fluorescent lightning and a growth cabinet with white LED lights. Relative water content  
541 measurements were done as previously described<sup>3336</sup>

542 **qRT-PCR analysis.**

543 Seeds were surface sterilized as described before<sup>2</sup> and grown in rhizotrons, 100 cm<sup>3</sup> pots, or  
544 on two types of 1% agar (Duchefa) media containing either 1x MS nutrients (Caisson) and 1%  
545 Sucrose, (termed ms media) or ¼x MS nutrients only (termed ms25 media). Both media were  
546 buffered using 0.5 g/L MES and pH was adjusted to 5.7 with KOH. All plants were grown  
547 together in a growth cabinet with LED lights under long day conditions (16h day/8h night).  
548 Root and shoot tissue was collected separately from individual plants at the end of the day  
549 (1 hour before the lights shut off) and at the end of the night (1 hour before lights came on).  
550 Three biological replicates were collected for each condition. RNA was extracted using the  
551 Plant RNA MiniPrepTM kit (ZYMO Research) according to manufacturer's instructions  
552 with on-column DNase treatment (Qiagen). cDNA was made using the iScript Advanced  
553 cDNA Synthesis for RT-qPCR kit (Bio-Rad) from 200 ng of total RNA. qRT-PCR was  
554 performed using a Fluidigm BioMarkTM 96.96 Dynamic Array IFC with the EvaGreen®  
555 (Bio-Rad) fluorescence probe according to the Fluidigm Advanced Development Protocol  
556 number 37. For the analysis, all the reactions with no amplification (Ct = 999) were set to  
557 the maximal Ct for that assay type. The two technical replicates were then averaged and  
558 dCt values calculated using AT3G07480, AT4G37830, At1g13320 and At1g13440 as reference  
559 internal controls. PCA plots were generated with Devium Web<sup>3437</sup> using dCt values. dCT  
560 values were calculated as dCT = CT~gene interest~ - mean(CT~reference gene~). Primers  
561 used are listed in file Supplement 8.

562 **Biological components.**

563   **Codon optimization of luciferases.** The following luciferases that emit light at different  
564   wavelengths were codon optimized for Arabidopsis (Genscript, Piscataway, NJ): LUC2: a  
565   yellow improved version (Promega, Madison, WI) of the original *Photinus pyralis* (firefly)  
566   LUC.

- 567   • Ppy RE8: a red variant<sup>3538</sup> of the *P. pyralis* thermostable variant Ppy RE-TS<sup>3639</sup>.
- 568   • CBG99: a green variant (Promega, Madison, WI) from yellow click beetle (*Pyrophorus*  
569   *plagiophthalmus*) luciferases.
- 570   • CBR: a red variant (Promega, Madison, WI) from yellow click beetle.

571   **Non-optimized luciferases.** We also used the following non-optimized luciferases:

- 572   • nanoLUC: a blue luciferase isolated from a deep sea shrimp<sup>14</sup>.
- 573   • venusLUC2: a venus-LUC2 fusion reported to show higher luminescence output than  
574   LUC2<sup>4245</sup>.
- 575   • A transposon containing the bacterial luciferase-containing LUX operon was integrated  
576   into the *Pseudomonas fluorescens* CH267<sup>1922</sup> genome by conjugation with *E. coli*  
577   *SM10pir* containing pUT-EM7-LUX<sup>3740</sup> and used to track root microbe colonization.  
578   For inoculation 9 DAS plants were inoculated with 2 mL of an overnight bacterial  
579   culture resuspended in 10 mM MgSO<sub>4</sub> and diluted to 0.01 OD.

580   **Generation of single-reporter transgenic plants.** We generated transcriptional fu-  
581   sions of all luciferases to constitutive promoters to examine the activity level and emission  
582   spectrum of each isoform. The *attL1-attL2* entry clones containing plant-codon optimized  
583   coding sequence of *LUC2*, *PpyRe8*, *CBG99* and *CBR* were synthesized by Genscript. A  
584   DNA fragment including the *UBQ10* promoter region and first intron was amplified from  
585   Col-0 genomic DNA with primers incorporating the attB1, attB4 combination sites at the  
586   5' and 3' respectively. The PCR product was then introduced into pDONR<sup>TM</sup> P4-P1R

587 (Invitrogen) through a classic Gateway BP-reaction. The resulting plasmid, the *attL1-attL2*  
588 entry clones with luciferase sequences, an empty *attR2-attL3\** entry clone and the destination  
589 vector dpGreenmCherry<sup>2</sup> were used to construct *ProUBQ10:LUC2o*, *ProUBQ10:PpyRE8o*,  
590 *ProUBQ10:CBG99o* and *ProUBQ10:CBrO* through Gateway LR reactions. The destination  
591 vector *dpGreenmCherry* contains a plasma membrane-localized mCherry coding sequence  
592 driven by the 35S promoter and is used as a selectable marker of transformation at the  
593 mature seed stage<sup>2</sup>. We used Golden Gate cloning and the destination vectors that we had  
594 generated before<sup>4316</sup> for the following fusions: *ProUBQ10:nanoLUC2*, *ProUBQ10:venusLUC*,  
595 *ProACT2:PpyRE8o*. Briefly, the different components of each construct were PCR amplified  
596 with complementary BsaI or SapI cutting sites, mixed with the destination vector in a single  
597 tube, digested with either BsaI or SapI, ligated with T4 DNA ligase, then transformed  
598 into E. coli Top10 cells and plated on LB antibiotic plates containing X-gal as previously  
599 described<sup>4316</sup>. Junction sites were confirmed by sequencing. We used pSE7 (Addgene  
600 ID #: pGoldenGate-SE7: 47676) as the destination vector of the *ProUBQ10:nanoLUC2*,  
601 *ProUBQ10:venusLUC* constructs and pMYC2 (Addgene ID #: pGoldenGate-MCY2: 47679)  
602 as the destination vector for *ProACT2:PpyRE8o*. Maps of all the vectors can be found in  
603 Supplement 8. *ProUBQ10:LUC2o* was transformed into Col-0, Bay and Sha accessions, the  
604 *tir1-1*<sup>3841</sup> mutant and the *miz1*<sup>3942</sup> T-DNA insertion line (SALK\_126928).

605 **Brachypodium distachyon.** The Arabidopsis plant-codon optimized Luciferase gene,  
606 *LUC2o*, was inserted into the monocot vector pANIC10 via Gateway cloning<sup>2831</sup>. *Brachy-*  
607 *podium distachyon* plants were transformed using the method of Vogel and Hill<sup>4043</sup>.

608 **Tomato.** The transcriptional fusion *ProeDR5:LUC2* was generated by cloning the  
609 *ProeDR5:LUC2* DNA fragment into the pBIB expression vector via restriction sites SalI  
610 and Acc65I. The eDR5 promoter is an enhanced version of DR5 containing 13 repeats of  
611 the 11-nucleotide core DR5 element<sup>4444</sup> and the pBIB expression vector contains an NPTII  
612 resistance gene under the control of the NOS promoter for use as a selectable marker during  
613 transformation. All tomato transformations were performed by the Ralph M. Parsons

614 Foundation Plant Transformation Facility (University of California, Davis).

615 **Generation of dual-reporter plants.** To generate dual-reporter plants expressing lu-  
616 ciferase isoforms that emit light with divergent emission spectra we used *ProACT2:PpyRE8o*  
617 as the root structural marker and ZAT12:LUC<sup>1821</sup> and DR5:LUC+<sup>1720</sup> lines that were  
618 transformed with the *ProACT2:PpyRE8o* construct. All constructs were transformed using  
619 a modified floral dip method as described in<sup>2</sup>.

620 To make the dual color tomato plants, the *Pro35S:PpyRE8o* transcriptional fusion was  
621 generated by putting the plant-codon optimized coding sequence described above into  
622 the pMDC32 expression vector through a Gateway LR reaction. The pMDC32 vector  
623 contains a hygromycin resistance gene under the control of the 35S promoter for use as a  
624 selectable marker during transformation. This construct was transformed into the transgenic  
625 *ProeDR5:LUC2* tomato line.

626 **In vivo emission spectra of plants constitutively expressing luciferase isoforms.**

627 To generate *in vivo* emission spectra of all constitutively expressed luciferases, seeds were  
628 sterilized and sown on MS plates as described before<sup>2</sup>. After 8 days, seedlings were treated  
629 with a 100 µM luciferin solution, incubated at room temperature for 3 hours and imaged using  
630 an IVIS Spectrum imaging system (Perkin Elmer, Waltham , MA) using 20 nm band-pass  
631 emission filters at the following wavelengths (in nm: 490-510, 510-530, 530-550, 550-570,  
632 570-590, 590-610, 610-630, 630-650, 650-670, 670-690, 690-710). Raw images were analyzed  
633 using Fiji and *in vivo* emission spectra were constructed. The full emission spectra of LUX  
634 and nanoLUC could not be constructed since the maximum of these two luciferases is below  
635 the lower band pass filter that were available.

636 **Imaging system.** We designed a custom imaging system (GLO1, Growth and Lumines-  
637 cence Observatory 1) optimized for imaging dual-reporter luciferase expression in our custom  
638 rhizotrons. The design was a joint effort with Bioimaging Solutions (San Diego, CA) who  
639 also built the system and wrote the acquisition software that drives all the mechanical parts

640 of the system. The system is composed by two 2048 x 2048 PIXIS-XB cameras (Princeton  
641 Instruments, Trenton, NJ) mounted on top of each other to capture two fields of view  
642 encompassing approximately two 15 x 15 cm areas corresponding to the top or bottom of  
643 the rhizotron. The cameras are fitted with a Carl-Zeiss macro lens. A filter wheel with space  
644 for four, 76.2 mm filters is positioned in front of the cameras and controlled by a stepper  
645 motor allowing for automated changing of the filter wheel position. We used two -542/50  
646 and 450/70- custom cut Brightline(R) band-pass filters (Semrock, Rochester, NY). In single  
647 color imaging mode, the filter wheel is operated without filters. Positioned in front of the  
648 filter wheel is a removable rhizotron holder mounted on a stepper motor. This stepper motor  
649 is also controlled by the GLO-1 software allowing automatic acquisition of images from both  
650 sides of the rhizotron sequentially. The whole imaging system is enclosed in a light-tight  
651 black box with a door that allows loading and un-loading of rhizotrons.

652 **Plant Imaging.** Around 50 mL of 300  $\mu$ M D-luciferin (Biosynth, Itasca, IL) was added to  
653 soil at the top of the rhizotron. In general 5 min exposures were taken per rhizotron, per  
654 side, per channel. For daily imaging experiments, plants were imaged at dawn (+/- 1 hr)  
655 to reduce possible effects on diurnal rhythms of keeping plants in the dark during imaging.  
656 Shoot images were taken using a Nikon D3100 camera.

657 **Image Preparation.** Four individual images are collected: top front, bottom front, top  
658 back and bottom back. Using an automated [ImageJ macro](#), a composite image is generated  
659 as follows: 1)To correct for differences in background values between the two cameras the  
660 mean background value of each image is subtracted from 200; 2) images are rotated and  
661 translated to control for small misalignments between the two cameras; 3) the top and  
662 bottom images of each side are merged; 4) the back image is flipped horizontally; 5) the  
663 front and back images are combined using the maximum values. When dual color images are  
664 acquired this operation is repeated for each channel. The final images produced are 16-bit  
665 depth and 4096 x 2048 pixels. The scale of the images is 138.6 pixels per cm. Considering  
666 that an *Arabidopsis* roots is 100  $\mu$ m this results in 1.39 pixels across an *Arabidopsis* root.

667 **GLO-RIA imageJ plug-in.** GLO-RIA uses a combination of existing tools to extract  
668 relevant root architecture features. Directionality is acquired using the [directionality plugin](#)  
669 from ImageJ. After the number of direction bins (we usually use bins of  $2\frac{9}{2}^o$ ) is defined by  
670 the user, a 5x5 sobel operator is used to derive the local gradient orientation. This orientation  
671 is then used to build a distribution of directions by assigning the square of the orientation  
672 into the appropriate bin. Instead of representing the total counts at each orientation a  
673 relative value is calculated by dividing the individual values at each bin by the total sum  
674 of the histogram (and multiplying by 100). Similar algorithms have been used to quantify  
675 dynamic changes in the plant cytoskeleton<sup>4245</sup>.

676 The Elliptic Fourier Descriptors are aquired using the [Fourier Shape Analysis plugin](#) on  
677 convex hull shape of the root system. Elliptic Fourier Descriptors have been used in numerous  
678 studies to analyse variations in shapes, notably in leaves (e.g.<sup>4346</sup>).

679 The shape analysis is inspired by RootScape<sup>4517</sup>. Due to the absence of fixed, recognisable  
680 structures in root system (that are required for the position of true landmarks), pseudo-  
681 landmarks are automatically extracted from the root systems. Shortly, the image is divided  
682 vertically at equidistant positions (with the number defined by the user) and for each of the  
683 image stripes, the minimum and maximum x coordinates are computed. The shape analysis  
684 is therefore able to discriminate root system with different vertical root distributions or  
685 global root system orientation (e.g. chemotropism) . The code source for the plugin, manual  
686 and sample images can be found in the [github repository](#) of the project.

687 Statistical analysis was performed in R<sup>4548</sup>. The tidyR<sup>4649</sup>, dplyr<sup>4649</sup>, gridExtra<sup>4750</sup>,  
688 shapes<sup>4851</sup>, geomorph<sup>4952</sup>, ggplot2<sup>5053</sup> and cowplot<sup>5154</sup> packages were used for data  
689 preparation, analysis and plotting. Final figure preparation was done in Inkscape.

690 **Data availability.** All the scripts and original data used to analyze and produce the images  
691 can be accessed in the Github repository of the project: [github.com/rr-lab/GLO-Roots](https://github.com/rr-lab/GLO-Roots). Raw  
692 files of all the images used in the paper are availabe in [Dryad](#).

<sub>693</sub> **Acknowledgements.**

<sub>694</sub> Work in the lab of JRD was funded by the Carnegie Institution for Science Endowment and  
<sub>695</sub> grants from the National Science Foundation (MCB-115795) and Department of Energy,  
<sub>696</sub> Biological and Environmental Research program (DE-SC0008769). RRA was supported by a  
<sub>697</sub> Carnegie Postdoc Fellowship and currently by Conacyt Ciencia Básica Joven Investigador  
<sub>698</sub> grant number (CB-2014-01-238101). GL was supported by the Belgian Fonds de la Recherche  
<sub>699</sub> Scientifique. JM was funded by the National Science Foundation (IOS-0820854). CH is  
<sub>700</sub> funded by MGH Toteston & Fund for Medical Discovery Fellowship grant 2014A051303  
<sub>701</sub> and NIH R37 grant GM48707 and NSF grant MCB-0519898 awarded to Frederick Ausubel,  
<sub>702</sub> and previously by the Gordon and Betty Moore Foundation through Grant GBMF 2550.01  
<sub>703</sub> from the Life Sciences Research Foundation. JV was funded by the Office of Biological and  
<sub>704</sub> Environmental Research, Office of Science, US Department of Energy, interagency agreements  
<sub>705</sub> DE-SC0001526 and DE-AI02-07ER64452. We thank Robert Mittler and Philip Benfey for  
<sub>706</sub> providing seeds of ZAT12:LUC and DR5:LUC+ respectively.  
<sub>707</sub> We also thank Neil Robbins and members of the Dinneny lab for critical review of the  
<sub>708</sub> manuscript and suggestions during the development of the project. We greatly appreciate  
<sub>709</sub> Tim Doyle at the Stanford Small Animal Imaging Facility for providing ´s advice in using  
<sub>710</sub> and help with luciferase-based imaging approaches.

<sub>711</sub> **Competing interests.**

<sub>712</sub> We do not have any competing interests that we are aware of.

<sub>713</sub> **Tables**

<sup>714</sup> **Tables.**

<sup>715</sup> **Table 1:** Luciferases used in this study.

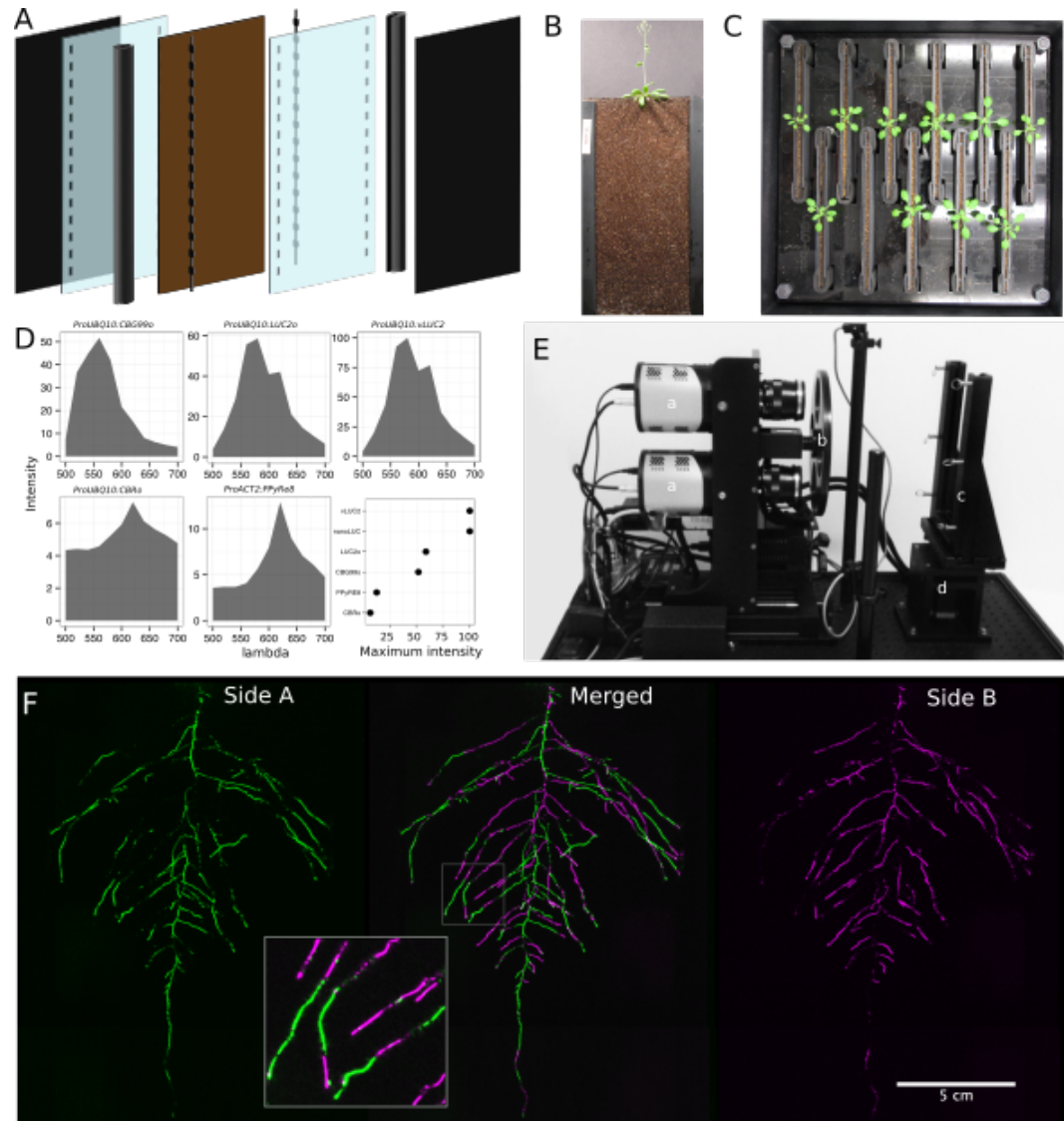
| Luciferase | Origin          | maximum wavelength | Substrate                                  |
|------------|-----------------|--------------------|--|
| Ppy RE8    | firefly         | 618                | D-luciferin                                |
| CBGRed     | click beetle    | 615                | D-luciferin                                |
| venus-LUC2 | FP + firefly    | 580                | D-luciferin                                |
| LUC(+)     | firefly         | 578                | D-luciferin                                |
| CBG99      | click beetle    | 537                | D-luciferin                                |
| lux operon | A. fischeri     | 490                | biosynthesis pathway encoded within operon |
| nanoLUC    | Deep sea shrimp | 470                | furimazine                                 |

<sup>716</sup> **Table 2:** list of root system features extracted using GLO-RIA.

| variable                      | unit |
|-------------------------------|------|
| projected area                | cm^2 |
| number of visible roots       | -    |
| depth                         | cm   |
| width                         | cm   |
| convex hull area              | cm^2 |
| width                         | cm   |
| feret                         | cm   |
| feret angle                   | °    |
| circularity                   | -    |
| roundness                     | -    |
| solidity                      | -    |
| center of mass                | cm   |
| Directionality                | °    |
| Euclidean Fourier Descriptors | -    |

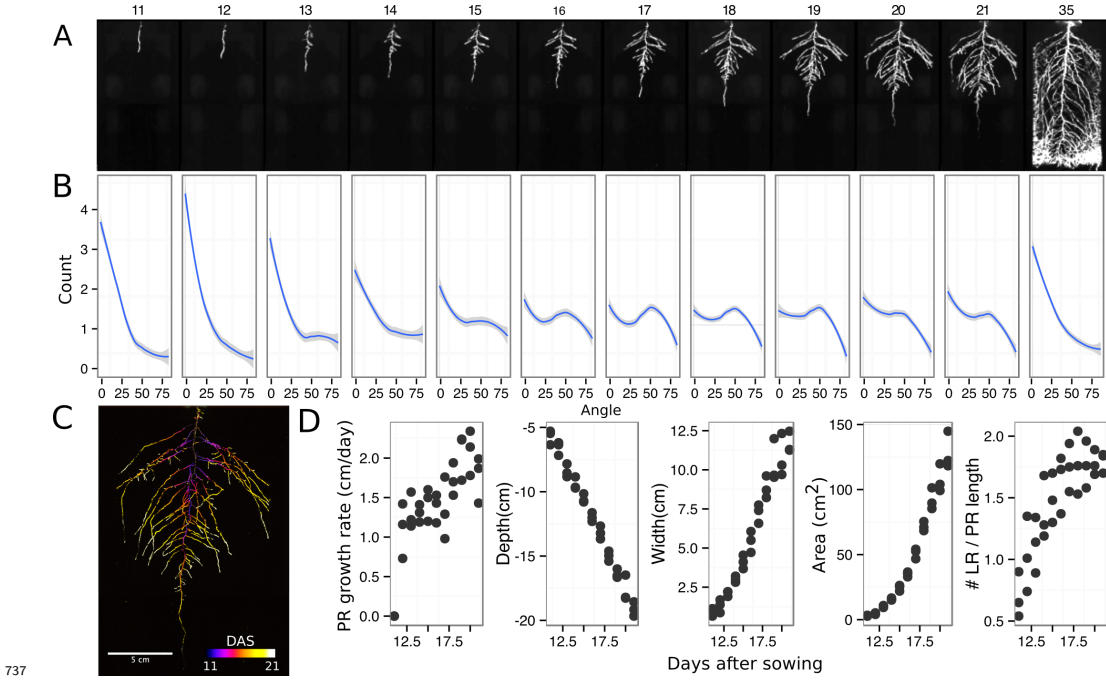
| variable         | unit |
|------------------|------|
| Pseudo landmarks | -    |

717 **Figures**



718  
719 **Figure 1. GLO-Roots growth and imaging systems** A) 3D representation of the  
720 different physical components of the rhizotron: plastic covers, polycarbonate sheets,  
721 spacers and rubber U-channels. Blueprints are provided in Supplementary material 1. In brown,  
722 soil layer. B) Thirty five day-old plant in rhizotron with black covers removed. C) Top view  
723 of holding box with eleven rhizotrons. D)In vivo emission spectra of different luciferases  
724 used in this study. Transgenic homozygous lines expressing the indicated transgenes were

725 grown on agar media for 8 days. Luciferin (300  $\mu$ M) was sprayed on the seedlings and plates  
726 were kept in the dark and then imaged for 2 s at wavelengths ranging from 500 to 700 nm.  
727 Five intensity values were taken from different parts of the roots of different seedlings and  
728 averaged. Relative maximum intensity values are indicated in the lower right graph. E)  
729 GLO 1 imaging system. The system is composed by two back illuminated CCD cameras  
730 (a) cooled down to -55 °C. A filter wheel (b) allows for spectral separation of the different  
731 luciferases. On the right, a rhizotron holder (c) is used to position the rhizotrons in front of  
732 the cameras. A stepper motor (d) rotates the rhizotron 180° to image both sides. F) A 21  
733 DAS plant expressing *ProUBQ10:LUC2o* was imaged on each of two sides of the rhizotron;  
734 luminescence signal is colorized in green or magenta to indicate side. In the middle of the  
735 panel, a combined image of the two sides is shown. The inset shows a magnified part of the  
736 root system. FW: fresh weight, PR: Primary root.



738 **Figure 2. Time-lapse imaging of root systems and quantification using GLO-**  
 739 **RIA.** A) Typical daily time-lapse image series from 11 to 35 DAS of a *ProUBQ10:LUC2o*  
 740 Col-0 plant. B) Directionality of the root system of plants in panel A calculated using the  
 741 directionality plugin implemented in GLO-RIA. C) Color coded projection of root growth  
 742 using the images in panel A. D) Primary root growth rate, depth, width, root system area  
 743 are automatically calculated from the convex hull, which is semi-automatically determined  
 744 with GLO-RIA. Lateral root number and number of lateral roots divided by the primary  
 745 root length were quantified manually. A Local Polynomial Regression Fitting with 95%  
 746 confidence interval (grey) was used to represent the directionality distribution curve. ( $0^\circ$  is  
 747 the direction of the gravity vector).

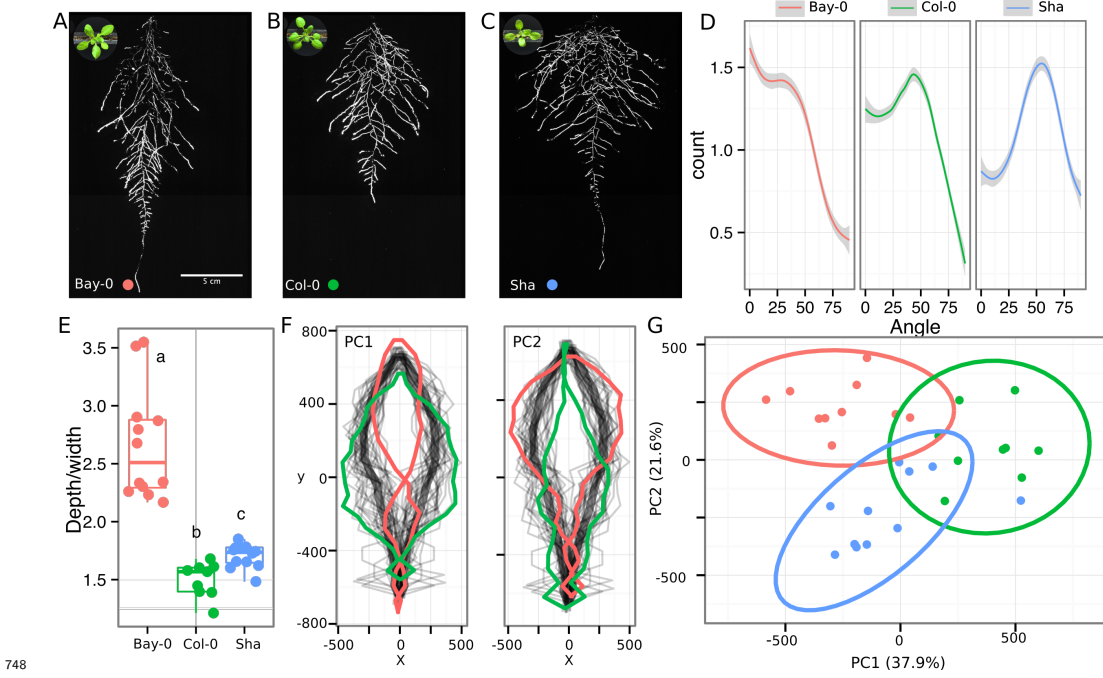
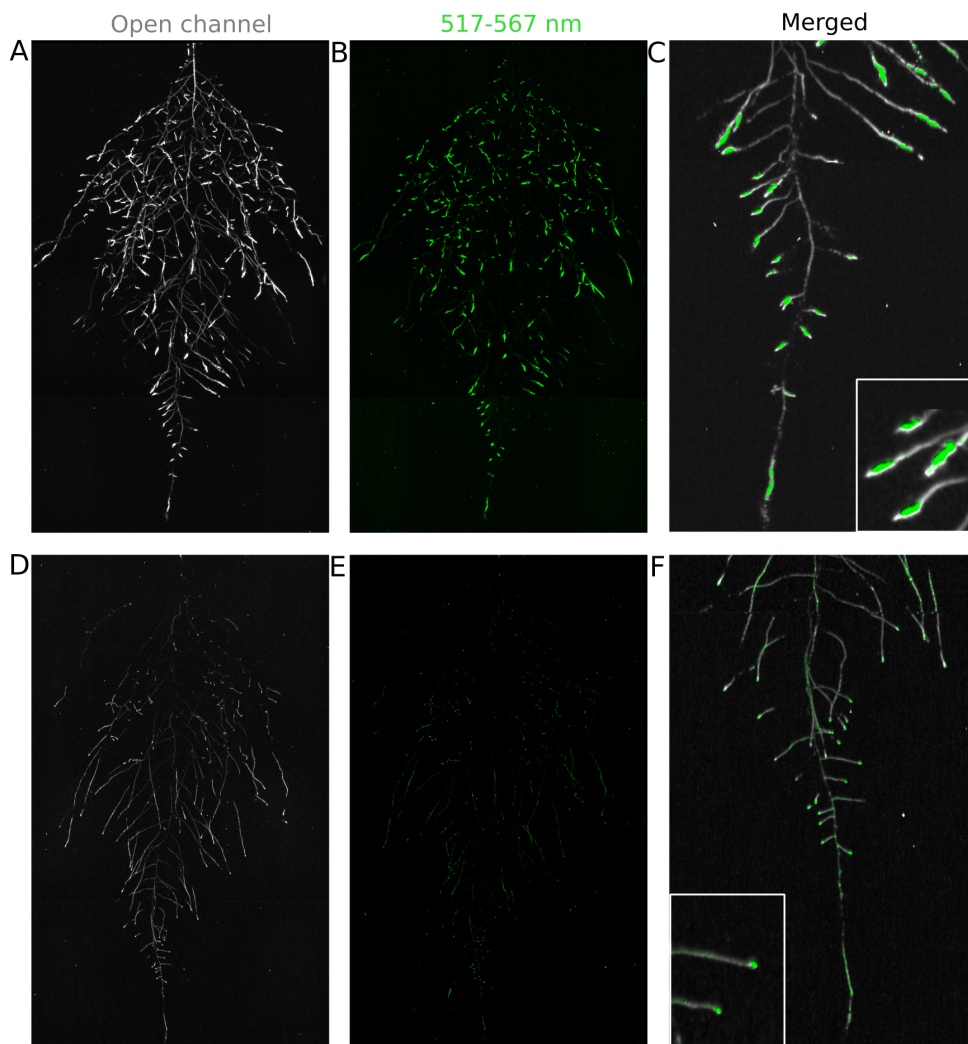


**Figure 3. Variation in root architecture between accessions of *Arabidopsis*.**

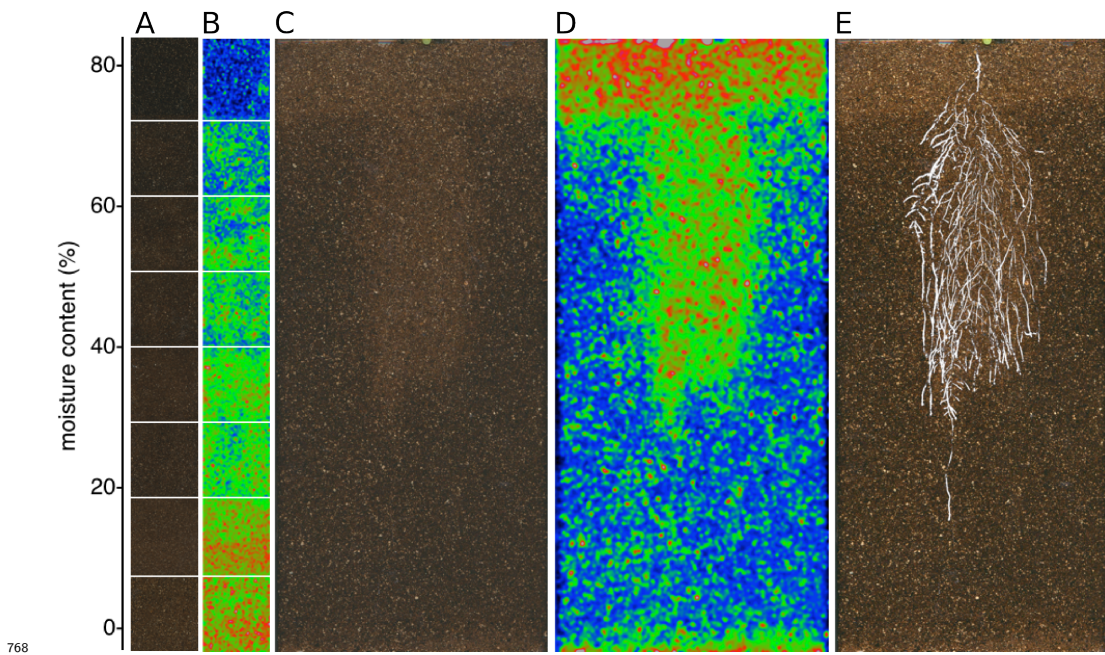
749 Representative root and shoot images of A) Bay-0, B) Col-0 and C) Sha accessions transformed  
 750 with `_ProUBQ10:LUC2o_` and imaged after 22 DAS. D) Directionality of the root systems,  
 751 with 95% confidence interval (grey) was used to represent the directionality distribution  
 752 curve. 0° is the direction of the gravity vector. Wilcoxon test analysis with  $p < 0.01$  was  
 753 used to test significant differences between the different accession ( $n = 9-12$  plants).  
 754 The first two Principal Components explaining 38% (PC1) and 22% (PC2) of the shape  
 755 variation are plotted. PC1 captures homogeneity of root system width along the vertical axis  
 756 and PC2 a combination of depth and width in top parts of the root system. Red and green  
 757 lines indicate -3SD and +3SD (Standard Deviations), respectively G) PC separation of the  
 758 different ecotypes using the PCs described in (F). A Local Polynomial Regression Fitting  
 759 with 95% confidence interval (grey) was used to represent the directionality distribution  
 760 curve. 0° is the direction of the gravity vector. Wilcoxon test analysis with  $p < 0.01$  was  
 761 used to test significant differences between the different accession ( $n = 9-12$  plants).



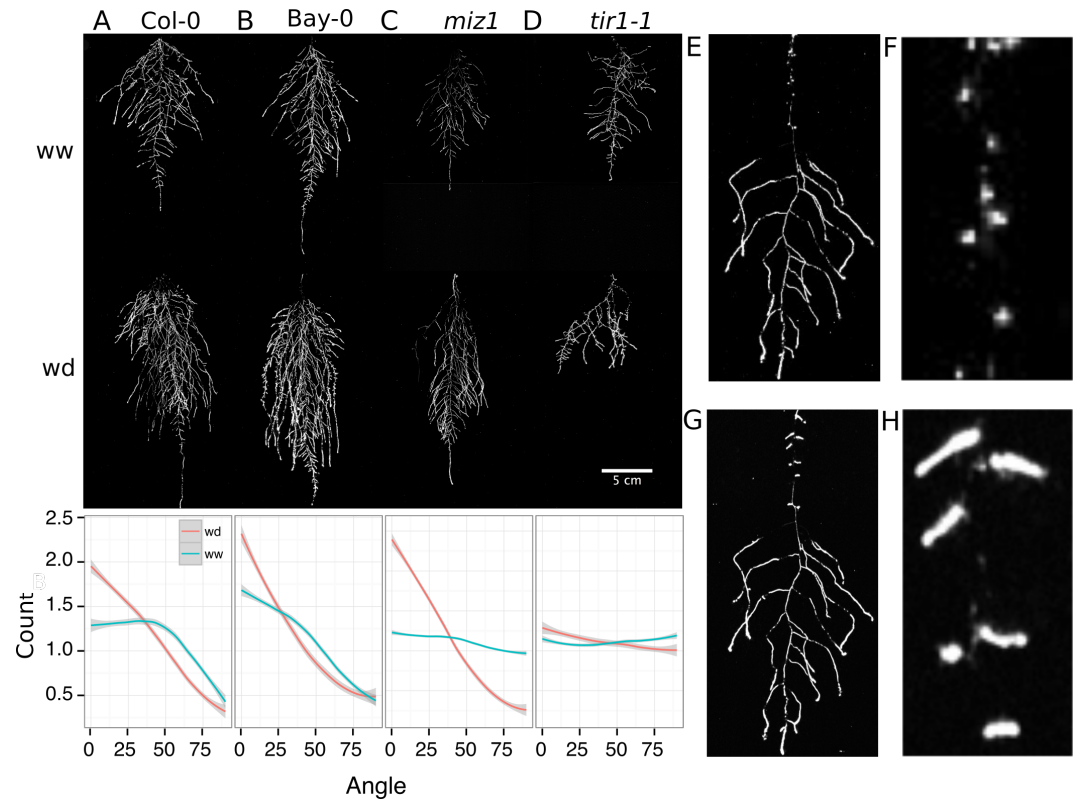
762

763 **Figure 4. Dual-color reporter visualization of structure and gene expression.**

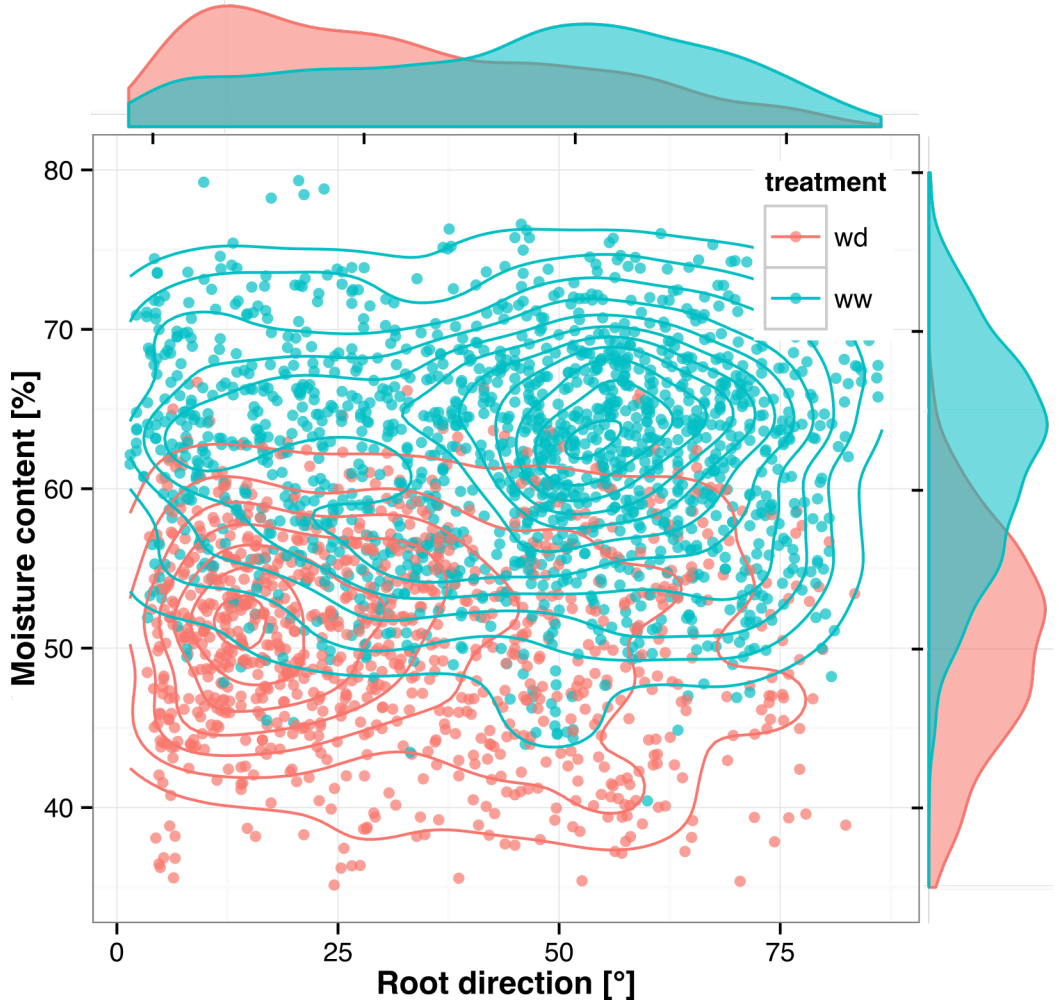
764 Images of whole root systems (A, D) or magnified portion of roots (C, F) at 22 DAS  
 765 expressing *ProDR5rev:LUC+* (green, A, B) or *ProZAT12:LUC* signal (green, D, E) with  
 766 skeletonized representation of roots generated using the *ProACT2:PpyRE8o* reporter  
 767 expression (in grey).



769 **Figure 5. Soil moisture and root architecture mapping in rhizotrons.** A) Com-  
 770 posite image showing regions of soil made from rhizotrons prepared with different moisture  
 771 levels. B) Differences in grey-scale intensity values were enhanced using a 16-color Look Up  
 772 Table (LUT). Brightfield image of soil in rhizotron (C) and converted using 16-color LUT to  
 773 enhance visualization of distribution of moisture (D) . E) Root system of a Bay-0 22 DAS  
 774 and subjected to water deprivation since 13 DAS. Root system visualized using luminescence  
 775 and overlaid on brightfield image of soil in (C).

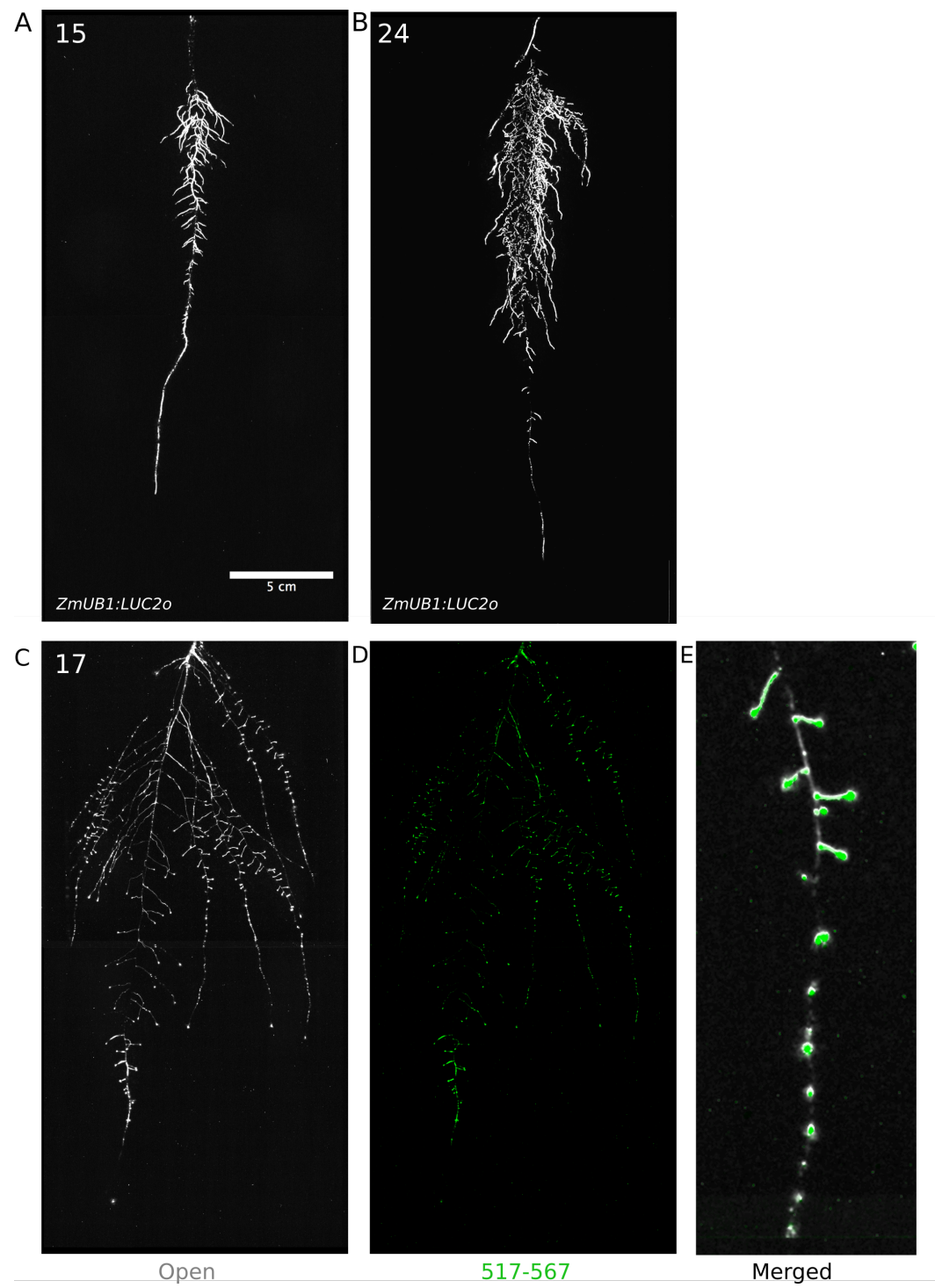


776 **Figure 6. Study of effect of water deficit on root system architecture.** A-D)  
 777 Root systems 22 DAS and exposed to water deficit 13 DAS onwards. Sample images of  
 778 well watered (left panels) and water deficit (right panels) root systems treated from 13  
 779 DAS and directionality (line graphs to left of images) for (A) Col-0 (B) Bay-0 (C) *miz1*  
 780 mutant and (D) *tir1-1*. E) Root system of a 22 DAS plant exposed to water deprivation  
 781 from 9 DAS onwards with magnified view of lateral root primordia (F). G) The same  
 782 root as in (E) 24 hours after rewetting and magnified view of lateral root primordia (H).  
 783 Kolmogorov-Smirnov test at  $p < 0.001$  was used to compare directionality distributions  
 784 between the different treatments and genotypes. A Local Polynomial Regression Fitting  
 785 with 95% confidence interval (grey) was used to represent the directionality distribution  
 786 curve.  $0^\circ$  is the direction of the gravity vector.  
 787



788

789 **Figure 7. Relationship between local soil moisture content and root growth**  
 790 **direction.** Data quantified from the time lapse series shown in [Video 2](#). Density plots shown  
 791 at periphery of graph for root direction (x-axis) and soil moisture (y-axis).  $0^\circ$  is the direction  
 792 of the gravity vector. Data represents 2535 root tips measured in a series encompassing 10  
 793 time points.



794 **Figure 8:** Roots of *Brachypodium distachyon* transformed with *ProZmUB1:LUC2o* and

<sup>796</sup> imaged at 15 (A) and 24 (B) DAS grown in control conditions. C) Open channel of 17 DAS  
<sup>797</sup> tomato plant transformed with *ProeDR5rev:LUC2o* and *Pro35S:PPyRE8o* D) Green channel  
<sup>798</sup> showing only *ProeDR5rev:LUC2o* E) Amplification of the open and green channel showing  
<sup>799</sup> increased expression of *ProeDR5rev:LUC2o* reporter in early-stage lateral roots.

800    **Videos**

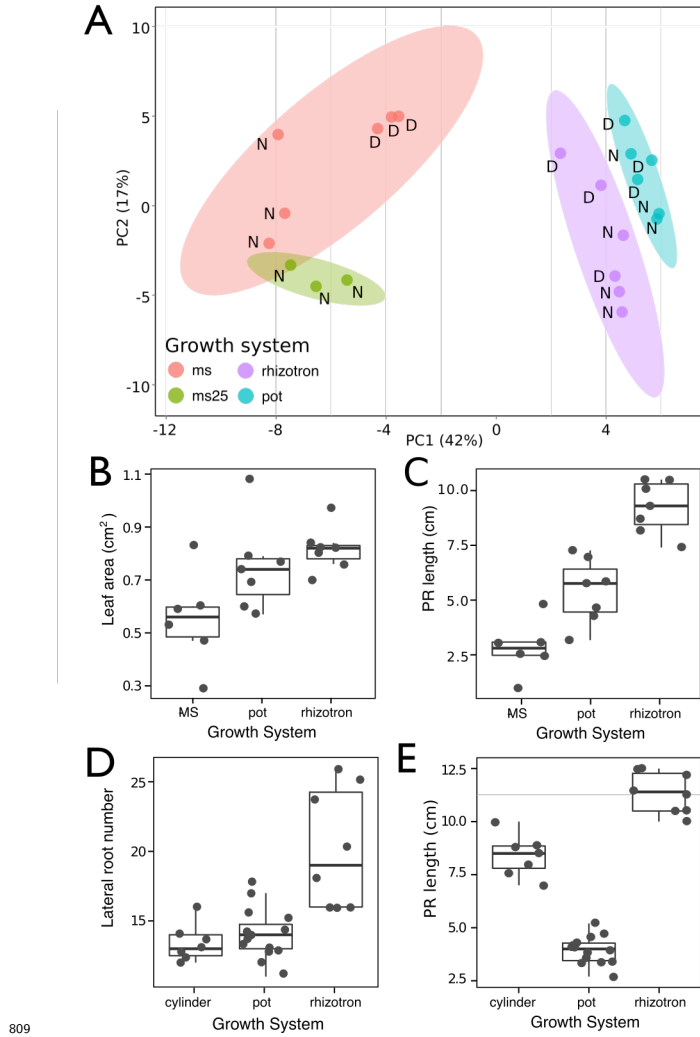
801    **Video 1** Time lapse from 11 to 21 DAS of a Col-0 plant expressing ProUBQ10:LUC2o  
802    grown in control conditions

803    **Video 2** Time lapse from 16 to 24 DAS of Col-0 plants expressing *ProUBQ10:LUC2o*  
804    growing in water deficient (left) and control (right) conditions. Plants were sown under  
805    control conditions and water deficit treatment started 11 DAS. Images were taken every day.

806    

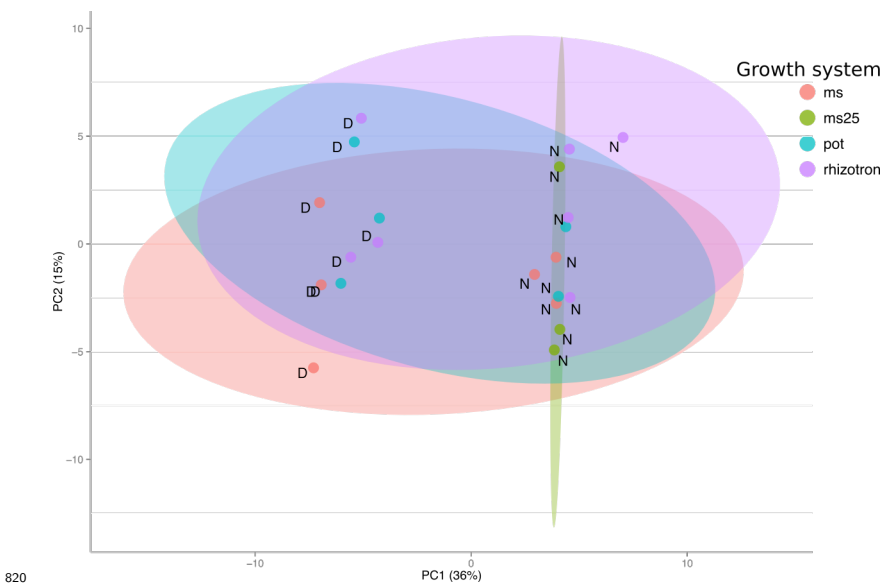
807      **Supplementary Material**

808      **Supplementary figures**



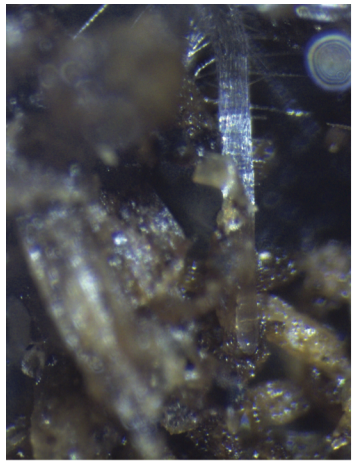
809  
810      **Figure 1-figure supplement 1. Effect of different growth systems on plant biol-**  
811      **ogy.** A) Principal Components Analysis (PCA) score plot of a set of 76 genes analyzed by  
812      qPCR from root samples of plants grown in MS plates, pots, and rhizotrons. After 15 DAS  
813      three plants were collected at the end of the day (D) and three were collected at the end of  
814      the night (N). (ms = plant grown in full ms and 1% sucrose, ms25 = plants grown in 25%  
815      of full ms) B) Lateral root number and G) primary root length of 18 DAS plants grown in

<sup>816</sup> 30 cm tall cylinders, pots and rhizotrons, all with a volume of 100 cm<sup>3</sup> (n = 6-12 plants).  
<sup>817</sup> D) Leaf area and E) primary root length of plants of the same age (15 DAS) as the ones  
<sup>818</sup> used for the qPCR experiment (n= 6-7). ANOVA analysis with p < 0.01 was used to test  
<sup>819</sup> significant differences between the different parameters.



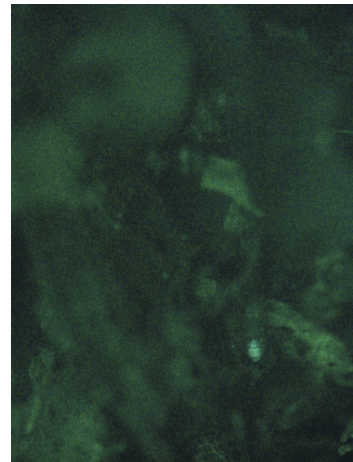
<sup>821</sup> \*Figure 1-figure supplement 2. PCA plot of shoots of the same samples analyzed in Figure 1.

<sup>822</sup> See Figure 1 for more details regarding experimental conditions used.



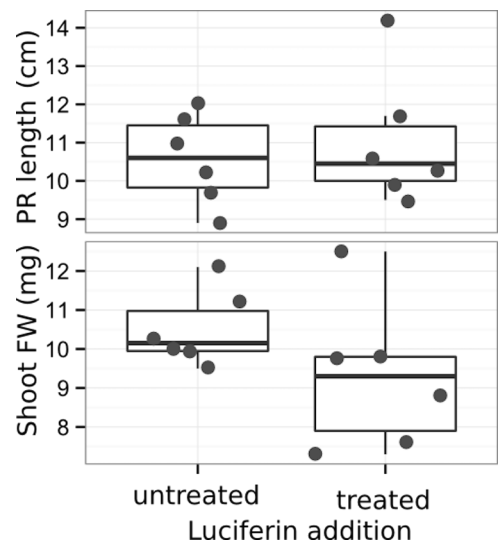
Brightfield

823



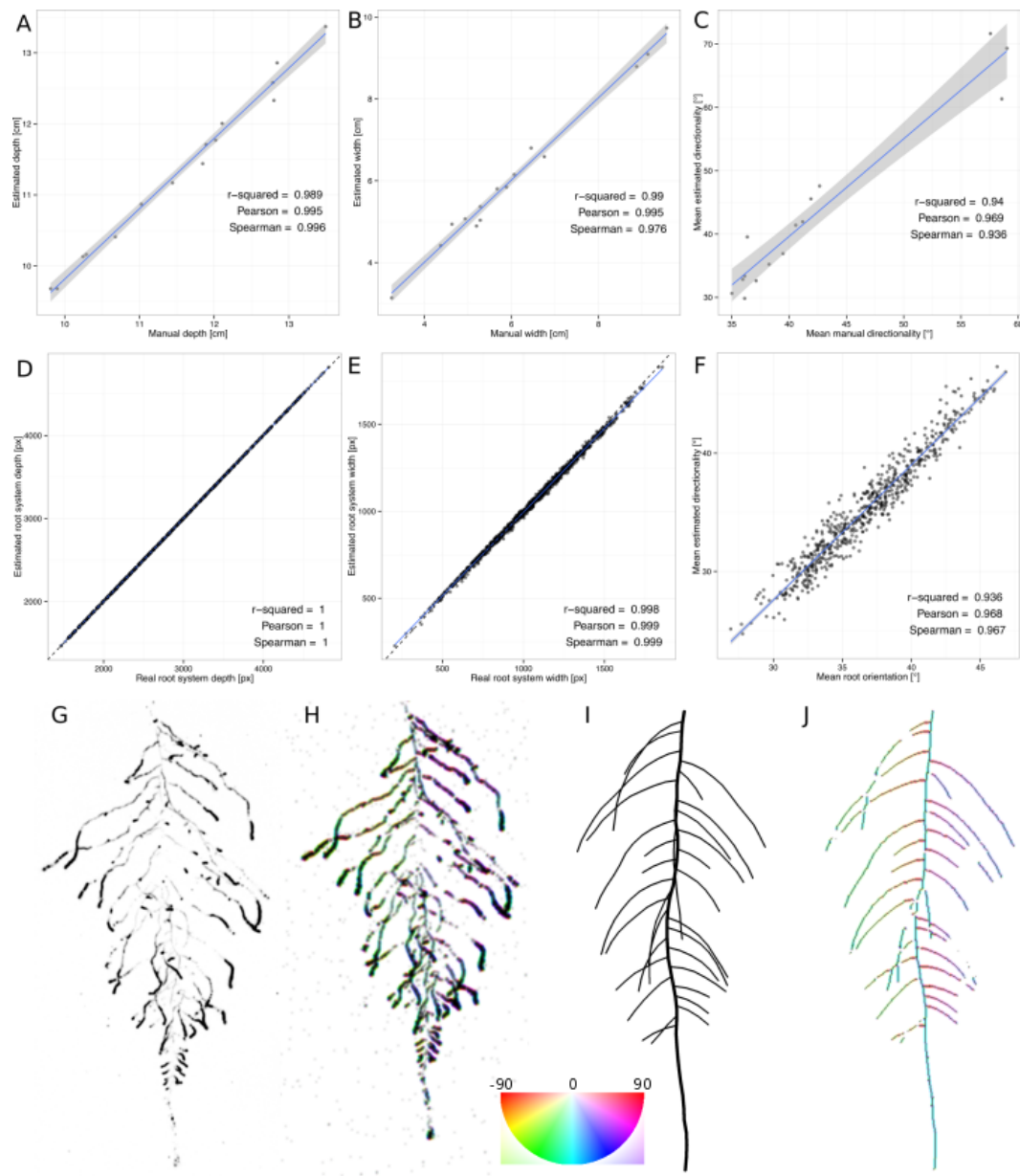
GFP

824 **Figure 1-figure supplement 3** Image of an Arabidopsis root in soil imaged with white  
825 light (brightfield) or epifluorescence.



826

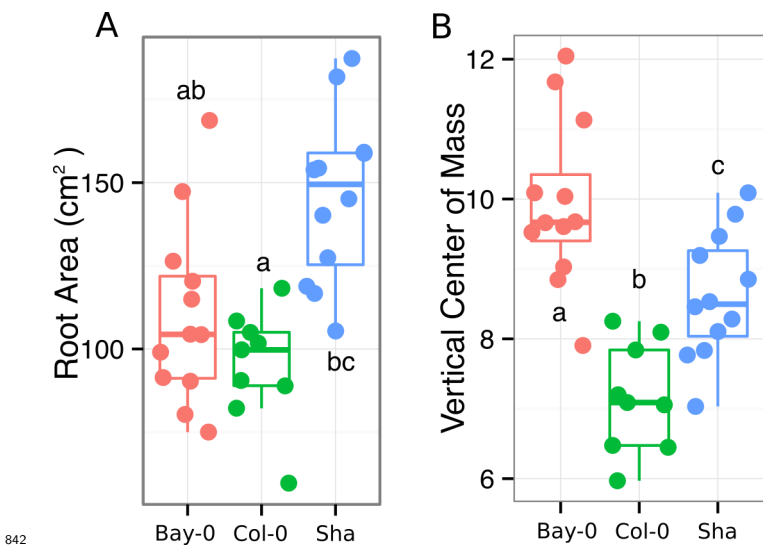
827 **Figure 1-figure supplement 4** Effect of luciferin addition on primary root length and  
 828 shoot size of 14 DAS seedlings that were either continuously exposed to 300  $\mu$ M luciferin  
 829 from 9 DAS after sowing or not.



830  
831 **Figure 1-figure supplement 5 GLO-RIA ground truth comparison. Tests of GLO-RIA**  
832 **were performed using two approaches. We first manually quantified root system depth (A)**  
833 **width (B) and average lateral root angle (C) in a set of 15 root systems corresponding**  
834 **to different *Arabidopsis* accessions. We also generated 1240 contrasting root systems**  
835 **using ArchiSimple and quantified root system depth (D) width (E) and directionality**

836 (F) using GLO-RIA. Example of a real (G) and ArchiSimple generated (H) root system  
837 and corresponding GLO-RIA determined directionality color-coded into the image (I, J).  
838 Absolute orientation angle values are taken before all calculations.

<sup>839</sup> **Figure 1-figure supplement data 1:** Two way ANOVA P-values comparing plants grown  
<sup>840</sup> in MS media vs. plants grown in soil (pots or rhizotrons) and plants collected at day or night.  
<sup>841</sup> We used p-value < 0.00065 threshold based on Bonferoni adjustment for multiple testing.



843 **Figure 3-figure supplement 1** A) root area, B) vertical center of mass of Bay-0, Col-0  
844 and Sha accessions.

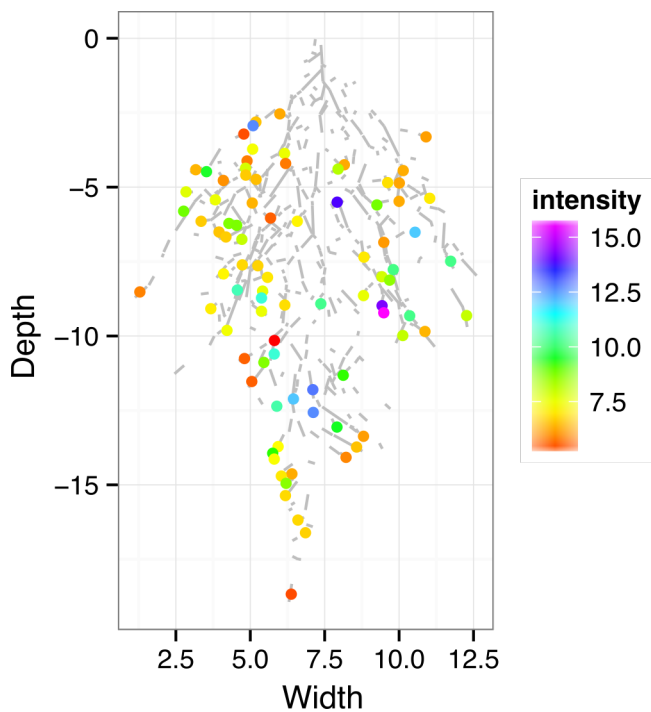
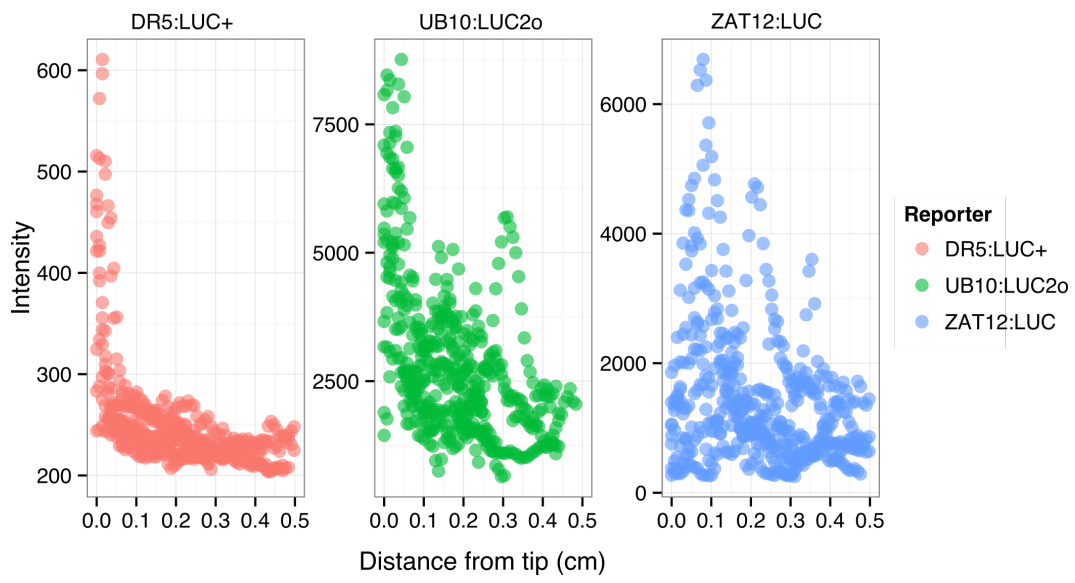


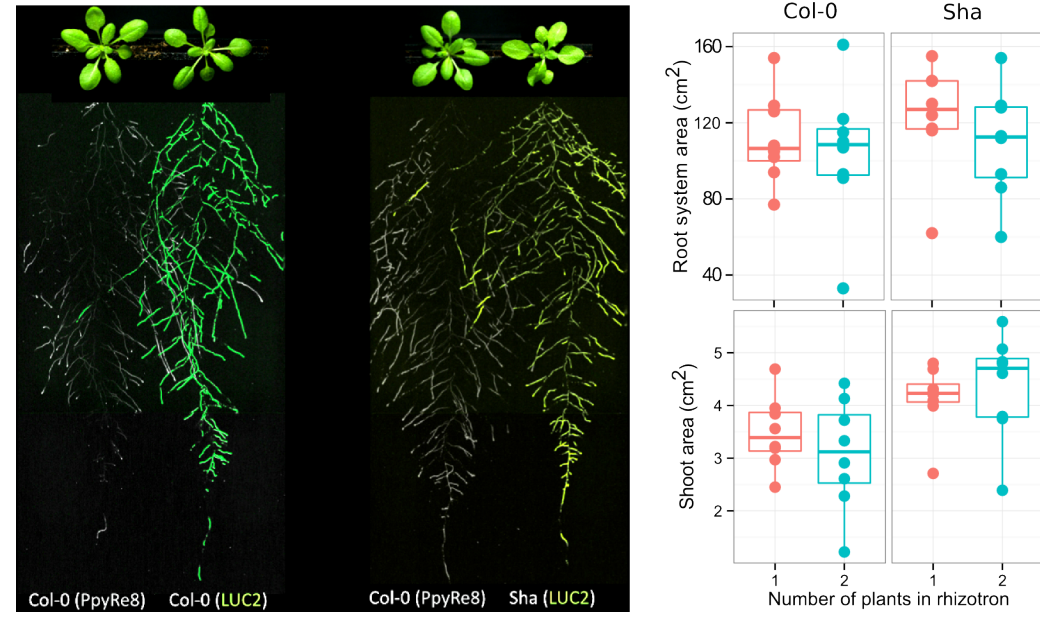
**Figure 4-figure supplement 1:**

845      ZAT12:LUC intensity and root segments automatically identified values along the root tip.  
 846  
 847      Data was manually obtained by obtaining the intensity profile of the first 0.5 cm from the  
 848      root tip of individual lateral roots. Ten lateral roots for each reporter were measured.  
 849



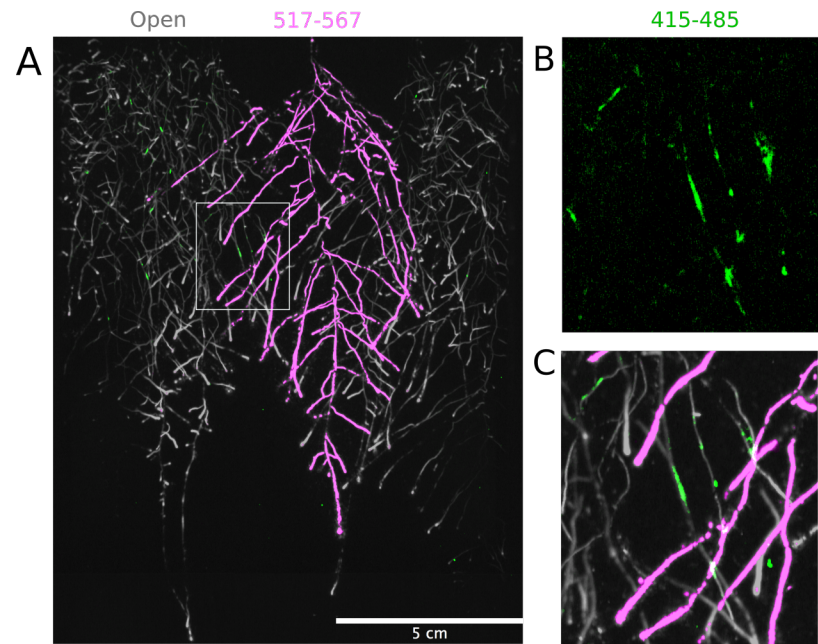
851 **Figure 4-figure supplement 2:** DR5:LUC+, UBQ10:LUC2o and ZAT12:LUC intensity  
 852 values along the root tip. Data was manually obtained by obtaining the intensity profile  
 853 of the first 0.5 cm from the root tip of individual lateral roots. Ten lateral roots for each  
 854 reporter were measured.

855

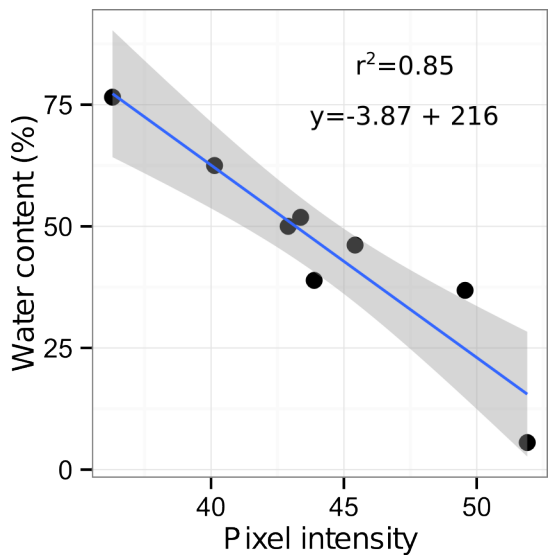


856  
857 **Figure 4-figure supplement 3.** Images of plants at 22 DAS growing in the  
858 same rhizotron and expressing different luciferases. A) Two Col-0 plants expressing  
859 *ProUBQ10:LUC2o* and *ProACT2:PPyRE8o* B) Col-0 plant expressing *ProACT2:PPyRE8o*  
860 and Sha plant expressing *ProUBQ10:LUC2o*.

861

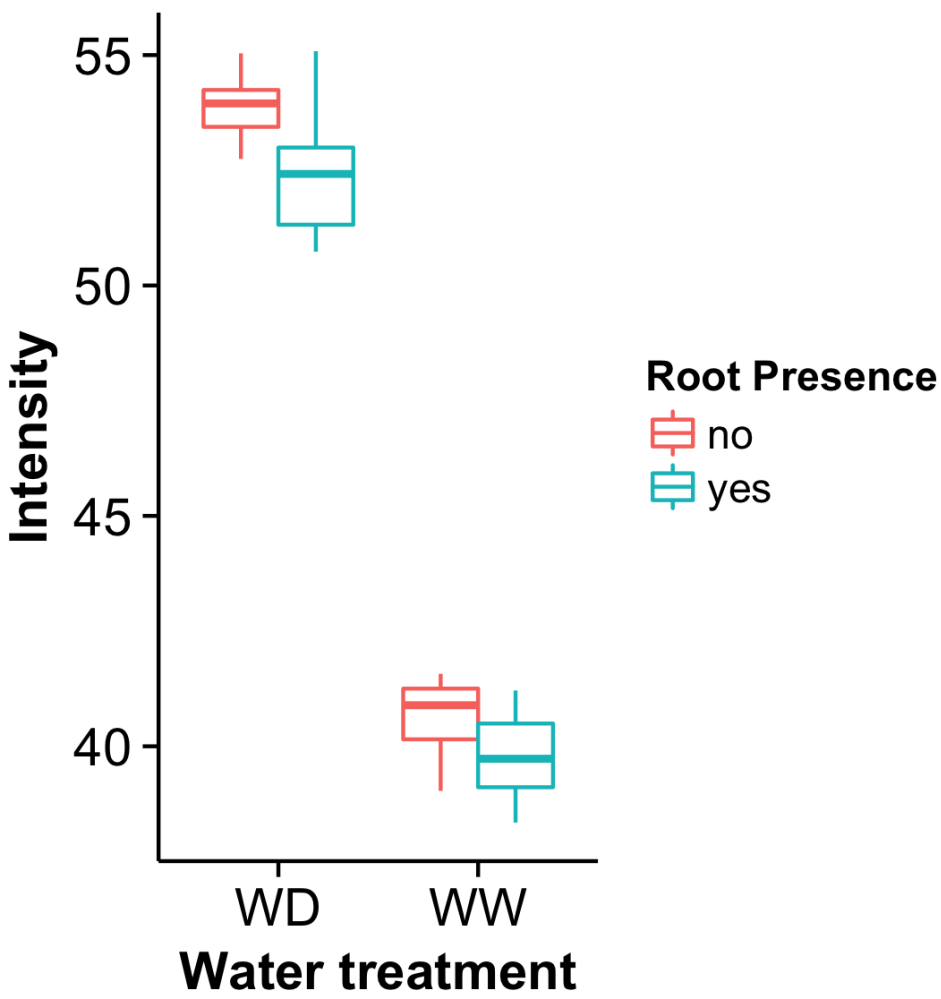


862  
863 **Figure 4-figure supplement 4. Three-reporter-based analysis of root-root-**  
864 **microbe interactions.** A) Image showing a 22 DAS *ProUBQ10:LUC2o* plant (magenta)  
865 grown in the same rhizotron with *ProACT2:PpyRE8o* plants (grey). Plants were inoculated  
866 with *Pseudomonas fluorescens* CH267 (green). Magnified portion of root systems colonized  
867 by *Pseudomonas fluorescens* showing *P. fluorescences* (B) only or all three reporters together  
868 (C).  
869



870      **Figure 5-figure supplement 1:** Moisture calibration curve. Rhizotrons with different  
871      levels of moisture were prepared and scanned to obtain readings of pixel intensity. Soil from  
872      rhizotrons was then weighed, dried down in an oven at 70 °C for 48 hours and percent water  
873      content quantified.  
874

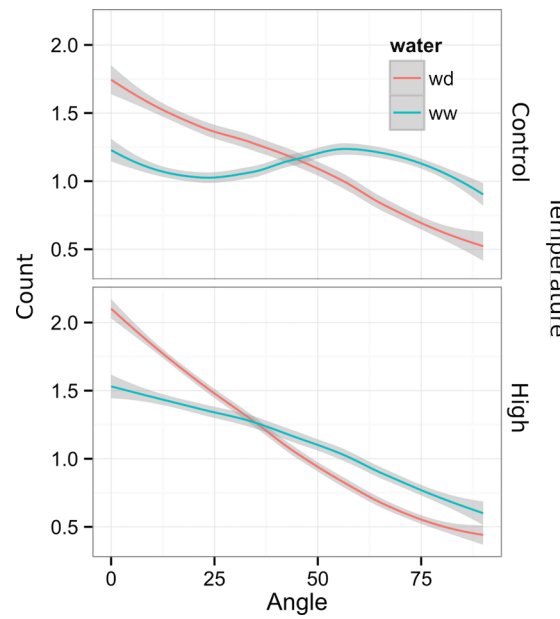
875



876

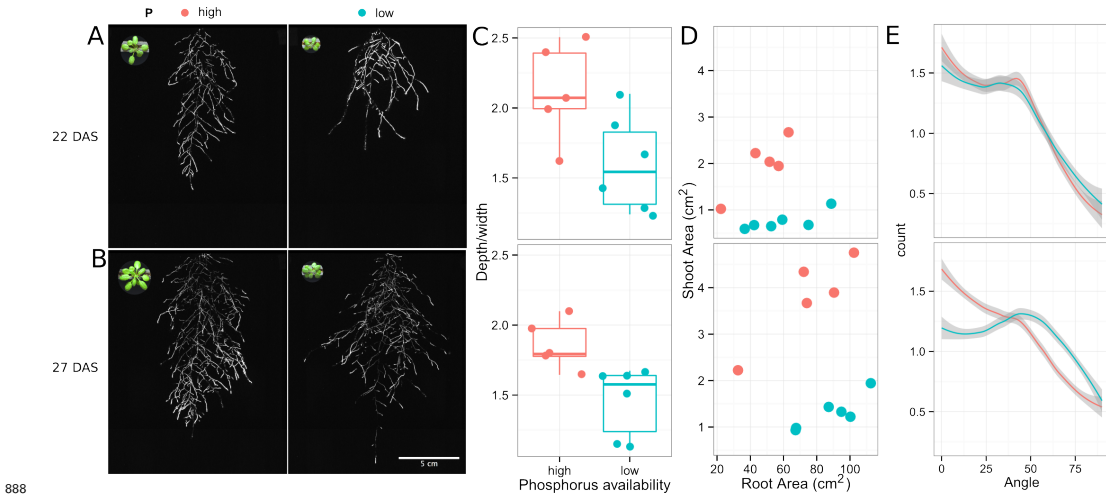
877 **Figure 5-figure supplement 2.** Comparison of soil intensity values between  
878 **areas of the rhizotron with or without the presence of roots, determined based**  
879 **on luminescence data.** Mean intensity values from 100 x 100 pixel squares samples of  
880 both areas were obtained from 10 different rhizotrons. Wilcoxon test analysis with  $p < 0.01$   
881 was used to test significant differences between areas with our without root presence.

882



883  
884 **Figure 6-figure supplement 1** Directionality analysis of roots of plants transferred to  
885 water deprivation conditions after 9 DAS and kept 22 °C (control temperature) and 29 °C  
886 (high temperature) until 22 DAS. (0° is the direction of the gravity vector).

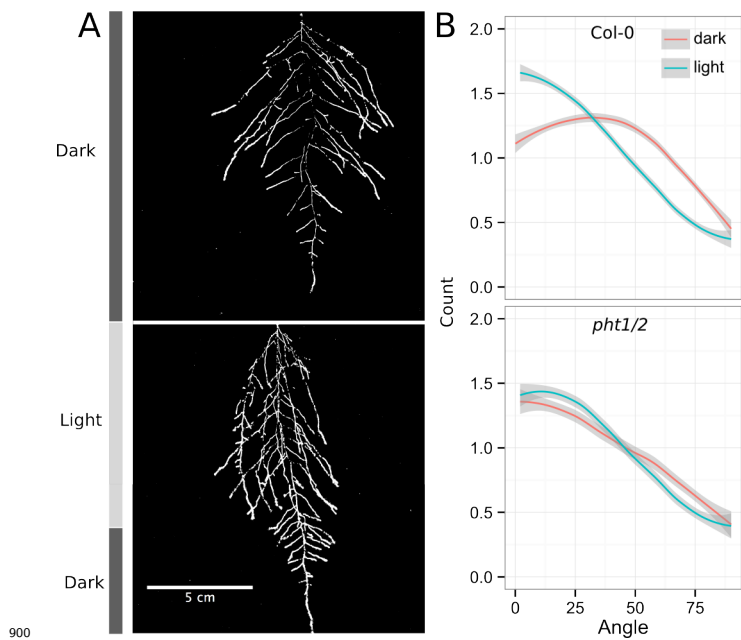
887



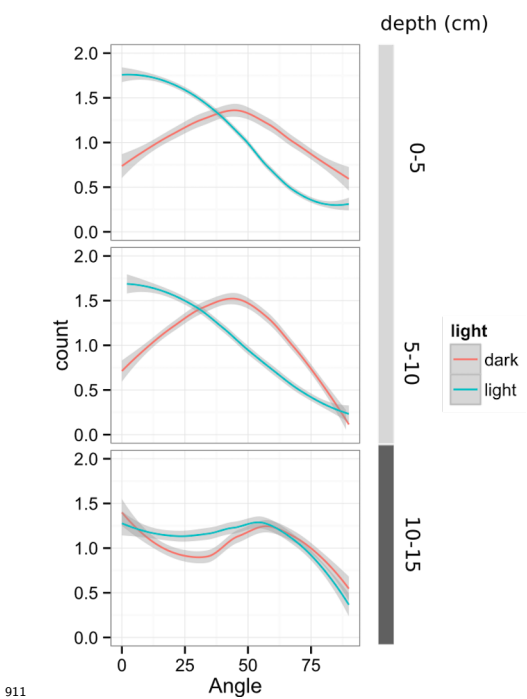
889 **Figure 6-figure supplement 2. Phosphorus deficiency response of root systems**

890 Shoot and root systems of *ProUBQ10:LUC2o* Col-0 plants growing in soil supplemented  
 891 with 1ml of 100  $\mu$ M P-Alumina (left) and 0-P-Alumina (right) 22 (A) or 27 (B) DAS. C)  
 892 Root depth/width ratio of 22 (top) and 27 (bottom) DAS plants. D) Scatter-plot showing  
 893 relationship between root and shoot system area at 22 (top) and 27 (bottom) DAS. E) Root  
 894 directionality distribution in plants 22 (top) and 27 (bottom) DAS. Anova analysis at  $p <$   
 895 0.01 was used to compare depth/width ratios in P treatments. Kolmogorov-Smirnov test at  
 896  $p < 0.001$  was used to compare directionality distributions between the different treatments.  
 897 A Local Polynomial Regression Fitting with 95% confidence interval (grey) was used to  
 898 represent the directionality distribution curve.(0° is the direction of the gravity vector).

899

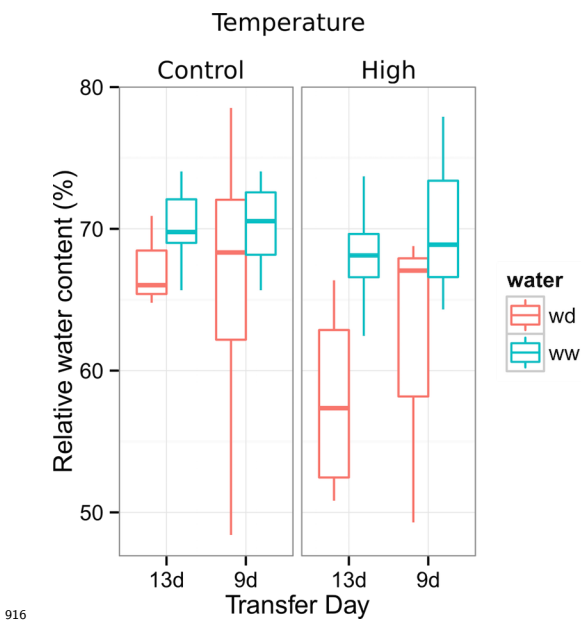


901 **Figure 6-figure supplement 3. Effect of light on root directionality.** A) Col-0 root  
902 systems shielded (top) or light exposed (bottom). After 9 DAS the top third of the rhizotron  
903 was exposed to light (indicated on the side with a light grey bar) and plants were imaged  
904 at 20 DAS. B) Directionality analysis of root systems shielded (red) or exposed (green) to  
905 light for Col-0 (top panel) or *pht1/2* double mutant (bottom panel). Between 4 and 6  
906 plants were analyzed per treatment. ANOVA analysis at  $p < 0.01$  was used to compare  
907 depth/width ratios in P treatments. Kolmogorov-Smirnov test at  $p < 0.001$  was used to  
908 compare directionality distributions between the different treatments. A Local Polynomial  
909 Regression Fitting with 95% confidence interval (grey) was used to represent the directionality  
910 distribution curve.(0° is the direction of the gravity vector).

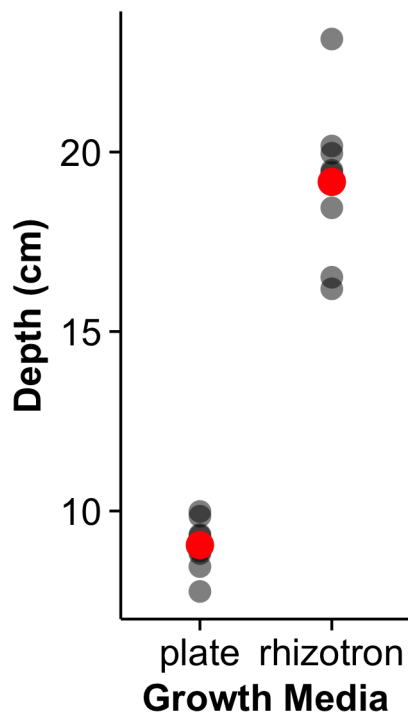


911 **Figure 6-figure supplement 4** Plots showing output of directionality analysis performed  
 912 at different depths (0-5, 5-10, 10-15 cm) in rhizotrons exposed to light or kept in the dark.  
 913  
 914 (0° is the direction of the gravity vector).

915



916     **Figure 6-figure supplement 5.** Leaf relative water content of 23 DAS plants that  
 917     were subjected to water deprivation (WD) after 9 or 13 DAS or kept under  
 918     well watered (WD) conditions. At 9 DAS half of the plants were kept under control  
 919     temperature conditions (22 °C) and the other half transferred to a 29 °C (high) chamber. n  
 920     = 6-8 plants.  
 921  
 922



923

924 **Figure 8-figure supplement 1** Depth of the primary root of *Brachypodium* plants grown

925 in rhizotrons or on gel-based media (n=8-11).

926

927 **Supplementary material**

928 **Supplemental Material 1**

929 Blueprints of the holders, clear sheets and spacers needed to built the rhizotrons. Additional  
930 details are provided in the materials and methods. Files are provided in Adobe Illustrator  
931 .ai and Autocad .dxf formats.

932 **Supplemental Material 2**

933 Primers used in the qPCR experiment.

934 **Supplemental Material 3**

935 Vector maps of all the constructs used in this work.

936 **Source data files**

937 Source data files used for building the following figures are provided:

938 [figure.csv](#)Figure 1-source data 1

939 [figure-B.csv](#)Figure 1-figure supplement 1-source data 1

940 [figure.csv](#)Figure 1-figure supplement 2-source data 1

941 [figure-F.csv](#)Figure 1-figure supplement 3-source data 1

942 [figure.csv](#)Figure 1-figure supplement 5-source data 1

943 [figure.csv](#)Figure 2-source data 1

944 [figure.csv](#)Figure 3-source data 1

945 [figure.csv](#)Figure 3-source data 2

946 [figure.csv](#)Figure 3-figure supplement 1-source data 1

947 [figure.csv](#)Figure 4-source data

948 [figure-G.csv](#)Figure 4-figure supplement 1-source data 1

949 [figure-G.tps](#)Figure 4-figure supplement 2-source data 1

950 [figure-B.csv](#)Figure 5-figure supplement 1-source data 1

951 [figure.csv](#)figure.csvfigure.csvfigure.csvfigure\_5\_figure\_supplement\_1.csv

952 [figure-D.csv](#)Figure 6-source data 1

953 [figure-C-D.csv](#)Figure 6-figure supplement 2-source data 1  
954 [figure-E.csv](#)Figure 6-figure supplement 3-source data 1  
955 [figure.csv](#)Figure 6-figure supplement 4-source data 1  
956 [figure.csv](#)Figure 6-figure supplement 5-source data 1  
957 [figure.csv](#)Figure 7-source data 1  
958 [figure.csv](#)[figure.csv](#)Figure 8-figure supplement 1-source data 1

959 

---

960    **References**

- 961    1.Dinneny, J. R. *et al.* Cell identity mediates the response of *Arabidopsis* roots to abiotic  
962    stress. *Science* **320**, 942–945 (2008).
- 963    2.Duan, L. *et al.* Endodermal ABA Signaling Promotes Lateral Root Quiescence during Salt  
964    Stress in Arabidopsis Seedlings. *Plant Cell* **25**, 324–341 (2013).
- 965    3.Lynch, J. P. & Wojciechowski, T. Opportunities and challenges in the subsoil: pathways to  
966    deeper rooted crops. *J. Exp. Bot.* **66**, 2199–2210 (2015).
- 967    4.Brady, N. C. & Weil, R. R. *Elements of the nature and properties of soils*. (Prentice Hall,  
968    2009).
- 969    5.Bao, Y. *et al.* Plant roots use a patterning mechanism to position lateral root branches  
970    toward available water. *Proc Natl Acad Sci* **111**, 9319–9324 (2014).
- 971    6.Tabata, R. *et al.* Perception of root-derived peptides by shoot LRR-RKs mediates systemic  
972    N-demand signaling. *Science* **346**, 343–346 (2014).
- 973    7.Rosquete, M. R. *et al.* An Auxin Transport Mechanism Restricts Positive Orthogravitropism  
974    in Lateral Roots. *Current Biology* **23**, 817–822 (2013).
- 975    8.Uga, Y. *et al.* Control of root system architecture by DEEPER ROOTING 1 increases rice  
976    yield under drought conditions. *Nat. Genet.* **45**, 1097–1102 (2013).
- 977    9.Postma, J. A. & Lynch, J. P. The optimal lateral root branching density for maize depends  
978    on nitrogen and phosphorus availability. *Plant Physiol.* **166**, 590–602 (2014).
- 979    10.[Laliberté, E. \*et al.\* How does pedogenesis drive plant diversity? \*Trends in ecology & evolution\* \*\*28\*\*, 331–340 \(2013\).](#)
- 981    11.[Tian, H., De Smet, I. & Ding, Z. Shaping a root system: regulating lateral versus primary  
982    root growth. \*Trends in plant science\* \*\*19\*\*, 426–431 \(2014\).](#)
- 983    12.[Schneider, C. A., Rasband, W. S. & Eliceiri, K. W. NIH Image to ImageJ: 25 years of  
984    image analysis. \*Nature methods\* \*\*9\*\*, 671–675 \(2012\).](#)

- 985 11.13. Meijon, M., Satbhai, S. B., Tsuchimatsu, T. & Busch, W. Genome-wide association  
986 study using cellular traits identifies a new regulator of root development in. *Nat. Genet.*  
987 **46**, 77–81 (2013).
- 988 12.14. Hall, M. P. *et al.* Engineered Luciferase Reporter from a Deep Sea Shrimp Utilizing  
989 a Novel Imidazopyrazinone Substrate. *ACS chemical biology* **7**, 1848–1857 (2012).
- 990 15. Hara-Miyauchi, C. *et al.* Bioluminescent system for dynamic imaging of cell and animal  
991 behavior. *Biochem. Biophys. Res. Commun.* **419**, 188–193 (2012).
- 992 13.16. Emami, S., Yee, M.-C. & Dinneny, J. R. A robust family of Golden Gate Agrobacterium  
993 vectors for plant synthetic biology. *Front. Plant Sc.* **4**, 339 (2013).
- 994 14. Hall, M. P. *et al.* Engineered Luciferase Reporter from a Deep Sea Shrimp Utilizing a  
995 Novel Imidazopyrazinone Substrate. *ACS chemical biology* **7**, 1848–1857 (2012).
- 996 15.17. Ristova, D. *et al.* RootScape: a landmark-based system for rapid screening of root  
997 architecture in Arabidopsis. *Plant Physiology* **161**, 1086–1096 (2013).
- 998 16.18. Lobet, G. *et al.* Root System Markup Language: toward a unified root architecture  
999 description language. *Plant Physiol.* **167**, 617–627 (2015).
- 1000 17.19. Pagès, L. *et al.* Calibration and evaluation of ArchiSimple, a simple model of root  
1001 system architecture. *Ecological Modelling* **290**, 76–84 (2014).
- 1002 20. Moreno-Risueno, M. A. *et al.* Oscillating gene expression determines competence for  
1003 periodic *Arabidopsis* root branching. *Science* **329**, 1306–1311 (2010).
- 1004 18.21. Miller, G. *et al.* The plant NADPH oxidase RBOHD mediates rapid systemic signaling  
1005 in response to diverse stimuli. *Science Signaling* **2**, ra45 (2009).
- 1006 19.22. Haney, C. H., Samuel, B. S., Bush, J. & Ausubel, F. M. Associations with rhizosphere  
1007 bacteria can confer an adaptive advantage to plants. *Nature Plants* **1**, 15051 (2015).
- 1008 20.23. Mandoli, D. F., FORD, G. A., WALDRON, L. J., NEMSON, J. A. & Briggs, W. R.  
1009 Some spectral properties of several soil types: implications for photomorphogenesis\*. *Plant  
1010 Cell Environ.* **13**, 287–294 (1990).

- 1011 21.24. Galen, C., Rabenold, J. J. & Liscum, E. Functional ecology of a blue light photoreceptor:  
1012 effects of phototropin-1 on root growth enhance drought tolerance in *Arabidopsis thaliana*.  
1013 *New Phytol.* **173**, 91–99 (2007).
- 1014 22.25. Moni, A., Lee, A. Y., Briggs, W. R. & Han, I. S. The blue light receptor Phototropin 1  
1015 suppresses lateral root growth by controlling cell elongation. *Plant Biology* 34–40 (2014).
- 1016 23.26. Yokawa, K., Kagenishi, T. & Baluška, F. Root photomorphogenesis in laboratory-  
1017 maintained *Arabidopsis* seedlings. *Trends Plant Sci.* **18**, 117–119 (2013).
- 1018 24.27. Lobell, D. B. *et al.* Greater Sensitivity to Drought Accompanies Maize Yield Increase  
1019 in the U.S. Midwest. *Science* **344**, 516–519 (2014).
- 1020 25.28. Ort, D. R. & Long, S. P. Limits on Yields in the Corn Belt. *Science* **344**, 484–485  
1021 (2014).
- 1022 26.29. Pacheco-Villalobos, D. & Hardtke, C. S. Natural genetic variation of root system  
1023 architecture from *Arabidopsis* to *Brachypodium*: towards adaptive value. *Philosophical  
1024 Transactions of the Royal Society of London B: Biological Sciences* **367**, 1552–1558 (2012).
- 1025 27.30. Watt, M., Schneebele, K., Dong, P. & Wilson, I. W. The shoot and root growth of  
1026 *Brachypodium* and its potential as a model for wheat and other cereal crops. *Functional  
1027 Plant Biol.* **36**, 960–969 (2009).
- 1028 28.31. Mann, D. G. J. *et al.* Gateway-compatible vectors for high-throughput gene functional  
1029 analysis in switchgrass (*Panicum virgatum* L.) and other monocot species. *Plant Biotechnol.  
1030 J.* **10**, 226–236 (2012).
- 1031 29.32. Pacheco-Villalobos, D., Sankar, M., Ljung, K. & Hardtke, C. S. Disturbed Local Auxin  
1032 Homeostasis Enhances Cellular Anisotropy and Reveals Alternative Wiring of Auxin-ethylene  
1033 Crosstalk in *Brachypodium distachyon* Seminal Roots. *PLoS Genet* **9**, e1003564 (2013).
- 1034 30.33. Buer, C. S., Wasteneys, G. O. & Masle, J. Ethylene modulates root-wave responses in  
1035 *Arabidopsis*. *Plant Physiology* **132**, 1085–1096 (2003).
- 1036 31.34. Blossfeld, S., Schreiber, C. M., Liebsch, G., Kuhn, A. J. & Hinsinger, P. Quantitative

- 1037 imaging of rhizosphere pH and CO<sub>2</sub> dynamics with planar optodes. *Annals of Botany* **112**,  
1038 267–276 (2013).
- 1039 **32.35.** Shaw, S. L. & Ehrhardt, D. W. Smaller, Faster, Brighter: Advances in Optical Imaging  
1040 of Living Plant Cells. *Annu. Rev. Plant Biol.* **64**, 351–375 (2013).
- 1041 **33.36.** Barr, H. & Weatherley, P. A re-examination of the relative turgidity technique for  
1042 estimating water deficit in leaves. *Aust. J. Biol. Sci* **15**, 413–428 (1962).
- 1043 **34.37.** Grapov, D. DeviumWeb: Dynamic Multivariate Data Analysis and Visualization  
1044 Platform.
- 1045 **35.38.** Branchini, B. R. *et al.* Red-emitting luciferases for bioluminescence reporter and  
1046 imaging applications. *Analytical Biochemistry* **396**, 290–297 (2010).
- 1047 **36.39.** Branchini, B. R. *et al.* Thermostable red and green light-producing firefly luciferase  
1048 mutants for bioluminescent reporter applications. *Analytical Biochemistry* **361**, 253–262  
1049 (2007).
- 1050 **37.40.** Lane, M. C., Alteri, C. J., Smith, S. N. & Mobley, H. L. T. Expression of flagella is  
1051 coincident with uropathogenic Escherichia coli ascension to the upper urinary tract. *Proc.  
1052 Natl. Acad. Sci. U.S.A.* **104**, 16669–16674 (2007).
- 1053 **38.41.** Ruegger, M. *et al.* The TIR1 protein of Arabidopsis functions in auxin response and is  
1054 related to human SKP2 and yeast grr1p. *Genes Dev* **12**, 198–207 (1998).
- 1055 **39.42.** Moriwaki, T. *et al.* Hormonal Regulation of Lateral Root Development in Arabidopsis  
1056 Modulated by MIZ1 and Requirement of GNOM Activity for MIZ1 Function. *Plant Physiol.*  
1057 **157**, 1209–1220 (2011).
- 1058 **40.43.** Vogel, J. & Hill, T. High-efficiency Agrobacterium-mediated transformation of Brachy-  
1059 podium distachyon inbred line Bd21-3. *Plant Cell Rep* **27**, 471–478 (2008).
- 1060 **41.44.** Covington, M. F. & Harmer, S. L. The Circadian Clock Regulates Auxin Signaling  
1061 and Responses in Arabidopsis. *Plos Biol* **5**, e222 (2007).

- 1062 42.45 Lindeboom, J. J. *et al.* A Mechanism for Reorientation of Cortical Microtubule Arrays  
1063 Driven by Microtubule Severing. *Science* **342**, 1245533–1–1245533–11 (2013).
- 1064 43.46 Chitwood, D. H. *et al.* A modern ampelography: a genetic basis for leaf shape and  
1065 venation patterning in grape. *Plant Physiology* **164**, 259–272 (2014).
- 1066 44.47 Iwata, H. & Ukai, Y. SHAPE: a computer program package for quantitative evaluation  
1067 of biological shapes based on elliptic Fourier descriptors. *The Journal of Heredity* **93**, 384–385  
1068 (2002).
- 1069 45.48 R Core Team. *R: A language and environment for statistical computing*. (R Foundation  
1070 for Statistical Computing, 2014). at <<http://www.R-project.org/>>
- 1071 46.49 Wickham, H. *Tidyr: Easily tidy data with spread() and gather() functions*. (2014). at  
1072 <<http://CRAN.R-project.org/package=tidyr>>
- 1073 47.50 Auguie, B. *GridExtra: Functions in grid graphics*. (2012). at <<http://CRAN.R-project.org/package=gridExtra>>
- 1074 48.51 Dryden, I. L. *Shapes: Statistical shape analysis*. (2013). at <<http://CRAN.R-project.org/package=shapes>>
- 1075 49.52 Adams, D. & Otarola-Castillo, E. Geomorph: An r package for the collection and  
1076 analysis of geometric morphometric shape data. *Methods in Ecology and Evolution* **4**, 393–399  
1077 (2013).
- 1078 50.53 Wickham, H. *Ggplot2: Elegant graphics for data analysis*. (Springer New York, 2009).  
1079 at <<http://had.co.nz/ggplot2/book>>
- 1080 51.54 Wilke, C. O. *cowplot: Streamlined Plot Theme and Plot Annotations for ggplot2*. (2015).  
1081 at <<http://cran.r-project.org/web/packages/cowplot/index.html>>